iScience

CellPress
OPEN ACCESS

Article

# Elucidating complex triplet-state dynamics in the model system isopropylthioxanthone

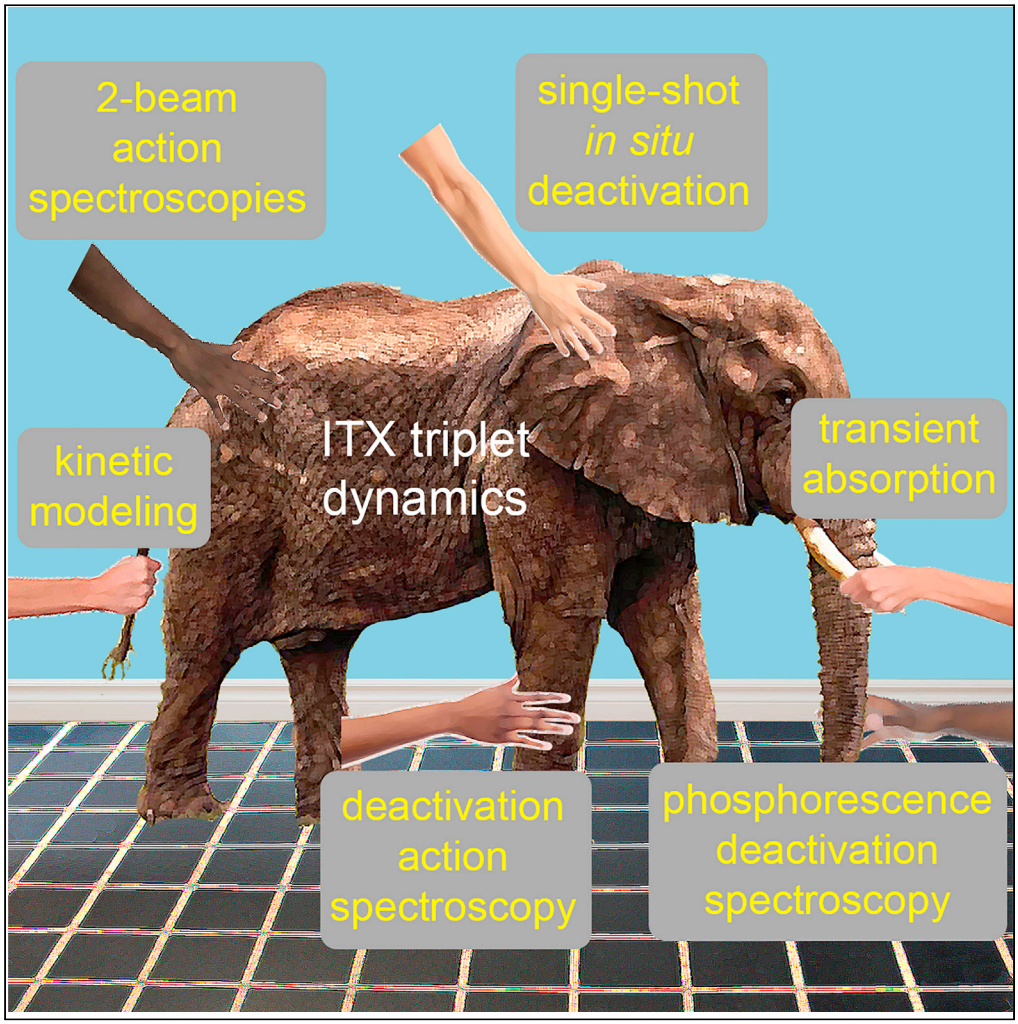


Nikolaos Liaros, Sandra A. Gutierrez Razo, Matthew D. Thum, ..., Daniel E. Falvey, Amy S. Mullin, John T. Fourkas

fourkas@umd.edu

## Highlights

Development of triplet-state dynamics probes to complement existing techniques

A detailed, mechanistic understanding of the photophysics of isopropylthioxanthone

Demonstration of self-deactivation during multiphoton excitation

Higher apparent nonlinearities can be detrimental to resolution

Liaros et al., iScience *25*, 103600
January 21, 2022 
https://doi.org/10.1016/j.isci.2021.103600

iScience

CellPress
OPEN ACCESS

Article

# Elucidating complex triplet-state dynamics in the model system isopropylthioxanthone

Nikolaos Liaros,[1] Sandra A. Gutierrez Razo,[1] Matthew D. Thum,[1,7] Hannah M. Ogden,[1] Andrea N. Zeppuhar,[1] Steven Wolf,[1,8] Tommaso Baldacchini,[2,9] Matthew J. Kelley,[2,10] John S. Petersen,[1,3] Daniel E. Falvey,[1] Amy S. Mullin,[1] and John T. Fourkas[1,4,5,6,11,*]

## SUMMARY

**We introduce techniques for probing the dynamics of triplet states. We employ these tools, along with conventional techniques, to develop a detailed understanding of a complex chemical system: a negative-tone, radical photoresist for multiphoton absorption polymerization in which isopropylthioxanthone (ITX) is the photoinitiator. This work reveals that the same color of light used for the 2-photon excitation of ITX, leading to population of the triplet manifold through intersystem crossing, also depletes this triplet population via linear absorption followed by reverse intersystem crossing (RISC). Using spectroscopic tools and kinetic modeling, we identify the reactive triplet state and a non-reactive reservoir triplet state. We present compelling evidence that the deactivation channel involves RISC from an excited triplet state to a highly vibrationally excited level of the electronic ground state. The work described here offers the enticing possibility of understanding, and ultimately controlling, the photochemistry and photophysics of a broad range of triplet processes.**

## INTRODUCTION

The vast majority of stable molecules have singlet ground states (Szabó and Ostlund, 1982). When such a molecule absorbs light, one electron is promoted to a higher unoccupied orbital. Because electronic transitions between states of different multiplicities are formally forbidden, the excited electronic state in such a transition generally must also be a singlet (Evans and Thompson, 1960). However, spin mixing due to weak spin-orbit coupling or hyperfine interactions can lead to a subsequent transition from the singlet to an optically "dark" triplet state, in a process known as intersystem crossing (ISC). Because electronic wave functions must be antisymmetric, the unpaired electrons in a triplet state cannot be in the same place at the same time. Thus, the triplet state for a given electronic configuration virtually always has a lower energy than the corresponding singlet excited state. The energy gap between the corresponding singlet and triplet states is usually well above thermal energy at room temperature. Thermally activated reverse intersystem crossing (RISC) from the lowest triplet state to the first excited singlet state has a low statistical probability when the energy gap is of this magnitude. The lowest triplet state can instead relax through processes such as phosphorescence (which also involves a spin flip, and therefore has an intrinsic lifetime that is considerably longer than that for a typical fluorescence transition), RISC to a vibrationally excited level of the ground singlet state, and collisional energy transfer. Alternatively, the triplet may undergo a chemical reaction.

There is a growing recognition that the ability to control triplet dynamics could lead to substantial advances in many photochemical and photophysical applications. For instance, trapping of population in dark triplet states reduces the fluorescence quantum yield of molecules and materials, which is a major issue in applications such as the development of efficient organic light-emitting diodes (Chang et al., 2013) and luminescent carbon nanotubes (Zhao and Mazumdar, 2004). Because of their metastable nature, triplet states can also be used to store energy; this capability plays an important role in applications such as the frequency upconversion of low-intensity light (Rauch and Knowles, 2018) and superresolved optical imaging (Bretschneider et al., 2007). Triplet states can also be harnessed for their chemical reactivity, as in photosensitization (Zhao et al., 2013) and photopolymerization (Chi et al., 2019; Harke et al., 2013).

Controlling triplet-state dynamics is a challenging problem. Any scheme for control must balance the influence of unimolecular phenomena that include ISC and RISC (Marian, 2012), heavy-atom effects

[1]Department of Chemistry & Biochemistry, University of Maryland, College Park, MD 20742, USA

[2]Newport Corporation, 1791 Deere Avenue, Irvine, CA 92606, USA

[3]imec, Kapeldreef 75, 3001 Leuven, Belgium

[4]Institute for Physical Science & Technology, University of Maryland, College Park, MD 20742, USA

[5]Maryland Quantum Materials Center, University of Maryland, College Park, MD 20742, USA

[6]Maryland NanoCenter, University of Maryland, College Park, MD 20742, USA

[7]Present address: Chemistry Division, Naval Research Laboratory, 4555 Overlook Avenue SW, Washington D.C. 20375, USA

[8]Present address: General Dynamics Information Technology, 5100 Springfield Pike, Dayton, Ohio 45431, USA, &Air Force Research Laboratory, Materials and Manufacturing Directorate, Functional Materials Division, Wright-Patterson AFB, Ohio 45433-7750, USA

[9]Present address: Edwards Lifesciences, One Edwards Way, Irvine, CA 92614, USA

[10]Present address: The Aerospace Corporation 2310 E. El Segundo Blvd., El Segundo, CA 90245-4609, USA

[11]Lead contact

*Correspondence: fourkas@umd.edu

https://doi.org/10.1016/j.isci.2021.103600

(Steiner and Winter, 1978), phosphorescence (Romanovskii et al., 2000), triplet absorption (Carmichael and Hug, 1986), thermally activated delayed fluorescence (Yang et al., 2017), and even coupling to photonic states in a cavity (Stranius et al., 2018). Bimolecular processes, such as triplet quenching (Patterson et al., 1970), triplet-triplet annihilation (Baldo et al., 2000), and singlet fission into two triplets (Smith and Michl, 2010), can also influence triplet dynamics. Developing a holistic understanding that encompasses such phenomena requires not only knowledge of the energies of both the singlet and triplet states of molecules, but also of the couplings among these states.

Laser spectroscopy has been a crucial tool for probing the rich photochemistry and photophysics of triplet states, and has provided a platform for fundamental studies on molecular electronic structure (Lower and El-Sayed, 1966), molecular reactions (Stromqvist et al., 2010), and the dynamics of electronic transitions (Buck et al., 2019). Despite considerable progress, the study of complex triplet-state dynamics remains challenging, and triplet electronic and spin properties are areas of intense research. Many triplet-associated phenomena are "dark," and as such, probing the nature of these processes often requires the use of multiple experimental techniques (Ge et al., 2015). Furthermore, the growing interest in multiphoton methods and applications in complex environments requires triplet probing methods that extend beyond the classical tool kit of phosphorescence, transient absorption, and electron paramagnetic resonance.

Spectroscopic tools that can probe triplet electronic transitions and dynamics in complex systems are critical for advancing the ability to control triplet states. Here, we introduce several such techniques, which we use in combination with existing methods to elucidate the rich triplet dynamics of a molecular system. As a representative system, we chose isopropylthioxanthone (ITX). Thioxanthones exhibit complex photophysics because their first two singlet excited states, one ($\pi,\pi^*$) and one ($n,\pi^*$), are quite close in energy, and in fact have an ordering that depends on the solvent (Angulo et al., 2010; Mundt et al., 2016). The same situation holds for the two lowest triplet states (Rai-Constapel et al., 2014; Villnow et al., 2014), for which again one is ($\pi,\pi^*$) and one is ($n,\pi^*$).

One reason for our particular interest in ITX stems from the fact that this substance is a photoinitiator that can be used in multiphoton absorption polymerization (MAP) (Fischer et al., 2010; Harke et al., 2012). MAP has attracted broad attention as a method for 3D photolithography at the nanoscale (Farsari and Chichkov, 2009; Fourkas, 2016a; LaFratta et al., 2007; Sugioka and Cheng, 2014). In its simplest implementation, MAP is performed in a negative-tone photoresist incorporating a radical photoinitiator that can be excited via the simultaneous absorption of two or more photons. Owing to the nonlinear optical nature of such excitation, MAP allows for the creation of lithographic features in the 100 nm size range using visible, or even near-infrared, light.

Outstanding resolution has been achieved in MAP by adapting approaches (Hell, 2007; Klar and Hell, 1999; Klar et al., 2000) from super-resolved fluorescence microscopy. In these advanced approaches to MAP, a negative-tone photoresist is excited using one beam of light and deactivated using a second beam (Fourkas, 2016b; Gan et al., 2013; Li et al., 2009; Liaros and Fourkas, 2019). By appropriate spatial shaping of these two beams, it is possible to improve both the feature size and resolution in MAP. Different mechanisms have been demonstrated for deactivation, and we will denote this general class of techniques as two-color lithography (2CL) (Fourkas and Petersen, 2014). A second reason for our particular interest is that ITX has been shown to be a useful initiator for 2CL (Chi et al., 2019, 2021; Fischer and Wegener, 2011; Harke et al., 2012, 2013; Mueller et al., 2014). Even though ITX is a Type II photoinitiator, this compound has been demonstrated to be able to initiate crosslinking of acrylates upon multiphoton excitation with pulsed 800 nm light in the absence of a coinitiator (Harke et al., 2012). This photochemistry has been shown to be suppressed by concurrent irradiation with a continuous-wave (CW) laser at either 532 nm or 630 nm (Fischer et al., 2010; Harke et al., 2013). It has been established that the mechanism of photodeactivation in ITX at these wavelengths is not stimulated emission (Wolf et al., 2011). To date, there has been no clear evidence regarding the details of the deactivation process, although it has been proposed that triplet states are involved (Chi et al., 2019, 2021; Harke et al., 2013).

Here, we demonstrate conclusively that excitation in ITX from the ground state to the first excited singlet state at wavelengths near 800 nm takes place via 2-photon absorption (2PA), even though the apparent number of photons absorbed is higher (Mueller et al., 2014). This behavior arises from the fact that the light at the excitation wavelength can also drive deactivation of the triplet state. Thus, although a higher order of nonlinear absorption can lead to improved feature sizes in MAP, in ITX the apparent greater number of photons is detrimental to resolution. By employing a combination of new and conventional spectroscopic

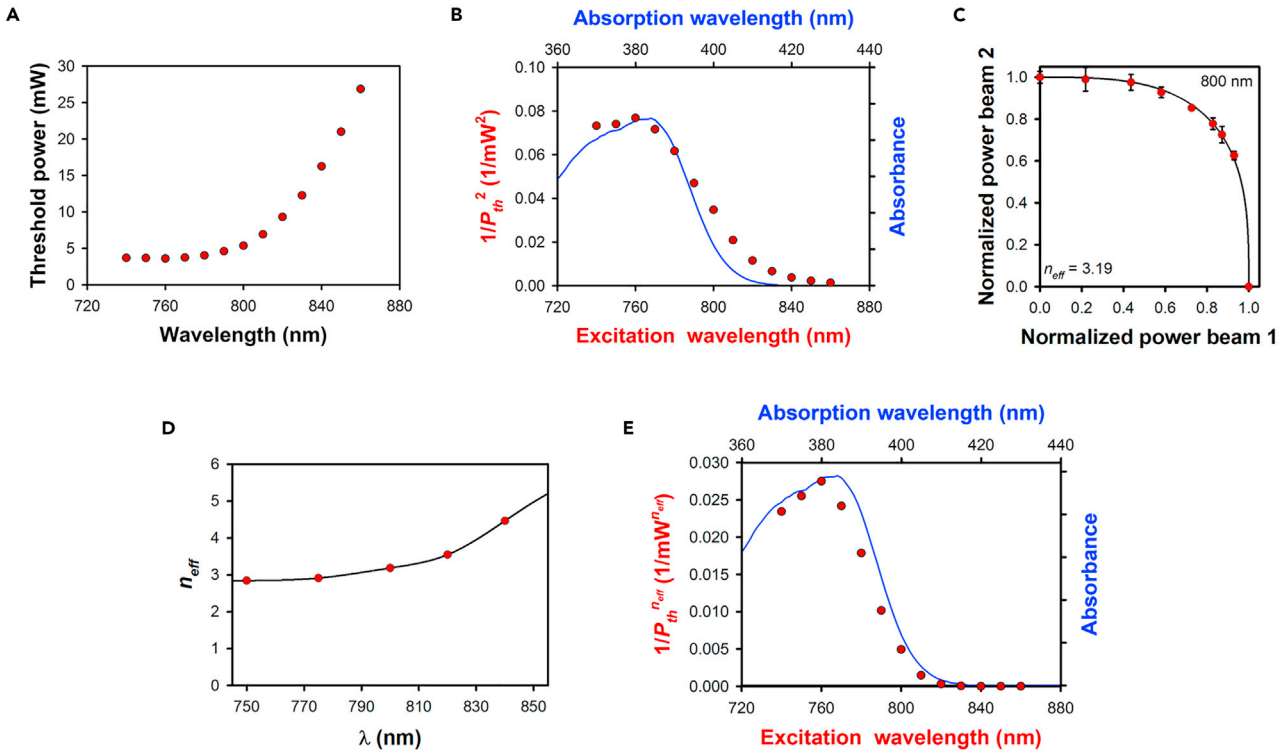


**Figure 1. Multiphoton exposure of an ITX/PETA photoresist**

(A) Threshold average power for initiation of multiphoton absorption polymerization measured at wavelengths from 750 nm to 850 nm.

(B) Polymerization action spectrum of the photoresist (symbols) and absorption spectrum of ITX in methanol (solid line).

(C) Representative 2-BIT data obtained at 800 nm (symbols) with the best-fit exponent (solid line). The error bars represent ±1 standard deviation, as determined by making multiple measurements.

(D) Dependence of $n_{eff}$ (symbols) on the excitation wavelength, with a cubic-spline fit (solid line).

(E) Linearized polymerization action spectrum taking into account $n_{eff}$ for each wavelength (symbols) and absorption spectrum of ITX in methanol (solid line).

tools, and by studying ITX both in photoresists and in solvents with similar polarities to the photoresists, we identify the triplet states and specific dynamics that are involved in the excitation, deactivation, and radical photochemistry of ITX.

## RESULTS

### Effective order of nonlinearity of ITX photoresists

ITX is generally considered to be a Type II photoinitiator, i.e., photoresists that use this material typically also include a coinitiator (Andrzejewska et al., 2006). However, it has been demonstrated that in some acrylic resins ITX can be used without a coinitiator, in a Type I process (Harke et al., 2012). Based on its absorption spectrum, ITX would appear likely to be excited by 2PA using light at wavelengths in the 800 nm range. However, experiments by Mueller et al. on a photoresist composed of ITX and pentaerythritol triacrylate (PETA) monomers suggested that excitation at 800 nm involves 4-photon absorption (Mueller et al., 2014). Such remarkably efficient 4-photon polymerization would be highly advantageous for high-speed, high-resolution MAP fabrication (Mueller et al., 2014). In contrast, Z-scan experiments have indicated that ITX in a solvent can be excited by 2PA at wavelengths in the 800 nm region (Kuebler et al., 1999). These results are not necessarily inconsistent, as promotion of an electron to the lowest excited singlet state of ITX might not lead to photopolymerization. On the other hand, the feature sizes reported for MAP for ITX-based photoresists with 800 nm excitation closely resemble what would be expected for 2PA. These seemingly contradictory results highlight the potential complexity of the determination of the true order of nonlinear absorption in multiphoton photoresists.

Figure 1A shows the power threshold for MAP measured at wavelengths in the range of 750 nm–850 nm in a photoresist composed of 1.5 wt% of ITX in PETA. The threshold power refers to the minimum power that is

required to form a cross-linked polymer using MAP. The cross-linked polymer has a different refractive index than the unexposed photoresist, and so can be observed by means of optical microscopy during fabrication. The threshold was determined by creating sets of lines at a constant height above the substrate surface at a stage velocity of 20 μm/s. The distance between adjacent lines was 2 μm, which is large enough to avoid proximity effects. The threshold power, $P_{th}$, for which polymerized lines were formed was determined visually (Baldacchini et al., 2004; Fischer et al., 2015).

An effective means of gaining insight into the order of nonlinearity in MAP is to determine the polymerization action spectrum, which is a plot of $P_{th}^{-n_{eff}}$ as a function of the excitation wavelength, where $n_{eff}$ is the effective order of nonlinear absorption (Baldacchini et al., 2004). Depicted in Figure 1B is a polymerization action spectrum calculated by assuming that $n_{eff} = 2$. The agreement between the polymerization action spectrum and the linear absorption spectrum of ITX at half the excitation wavelength is strong evidence that photoinitiation in this range of wavelengths is a 2-photon process.

We measured the effective order of absorption, $n_{eff}$, as a function of excitation wavelength to explore the discrepancy between the actual order of nonlinear absorption, which is 2, and the higher value of the effective order of absorption reported previously (Mueller et al., 2014). We employed the 2-beam initiation threshold (2-BIT) method (Tomova et al., 2016), a type of 2-beam action (2-BA) spectroscopy (Liaros et al., 2018a, 2018b), to perform *in situ* measurements of $n_{eff}$ in the ITX/PETA photoresist. In 2-BIT, two temporally interleaved, spatially overlapped pulse trains are used to expose a multiphoton photoresist (Figure S1). Pairs of irradiances that together provide the threshold exposure are measured. Data obtained with this technique obey the relation

$$\overline{P}_1^{n_{eff}} + \overline{P}_2^{n_{eff}} = 1, \qquad \text{(Equation 1)}$$

where the overbars indicate normalization of the average excitation power for each beam to the threshold power for that beam alone. A significant advantage of 2-BIT over other approaches for measuring the order of nonlinearity of photoresists is that important parameters that can change the measured value of $n_{eff}$, such as the exposure time and the repetition rate, are kept constant (Liaros and Fourkas, 2021).

Representative 2-BIT data for the ITX/PETA photoresist for 800 nm excitation are shown in Figure 1C. The best-fit $n_{eff}$ for these data is 3.19 $\pm$ 0.05. The data were obtained at a stage velocity of 20 μm/s. Although the value of $P_{th}$ depends on the stage velocity, the measured value of $n_{eff}$ was insensitive to velocity in the tested range of 10 μm/s to 40 μm/s. In Figure 1D, we plot $n_{eff}$ as a function of the excitation wavelength. The corresponding 2-BIT data and fits at each wavelength are shown in Figure S2. As seen in Figure 1D, $n_{eff}$ depends on the excitation wavelength, ranging from 2.85 $\pm$ 0.05 at 750 nm to 4.47 $\pm$ 0.16 at 840 nm. It is notable that the measured exponents take on non-integer values, which is often assumed to be indicative of mixed contributions from different orders (Fischer et al., 2015; Mueller et al., 2014; Yang et al., 2019). However, it is not plausible that the average order of nonlinear absorption should change so radically over such a small range of excitation wavelengths, given the details of the linear absorption spectrum of ITX and the fact that higher-order absorption should be a considerably weaker process. We have previously introduced a method to determine whether 2-BA data arise from a specific pair of orders of absorption (Cohen and Fourkas, 2019). The 2-BIT data for ITX do not fit well to either 2-photon plus 3-photon or 2-photon plus 4-photon absorption, as shown for the case of the 750 nm data in Figure S3.

To estimate the dependence of $n_{eff}$ on excitation wavelength, the data in Figure 1D were fit with a cubic spline (solid line in Figure 1D) to determine $n_{eff}(\lambda)$ in the range $\lambda$ = 750 nm–850 nm. Figure 1E shows a "linearized" polymerization action spectrum. To determine the wavelength axis, we assumed, as in Figure 1B, that the true order of nonlinear absorption over this wavelength range is 2, and we plot $P_{th}^{-n_{eff}(\lambda)}$ as a function of the excitation wavelength. The agreement between the linearized action spectrum and the absorption spectrum at half of the 2PA excitation wavelength is striking. This analysis indicates that polymerization occurs solely through a 2PA process throughout this range of wavelengths. The slight deviation between the linearized action spectrum and the linear absorption spectrum is attributed to the solvatochromic shift being different for ITX in monomers (for the action spectrum) and in methanol (for the absorption spectrum). The questions we now address are (1) Why are the measured exponents higher than 2? and (2) Why does $n_{eff}$ depend strongly on the excitation wavelength? From Figures 1D and 1E, it is also clear that weaker 2PA (i.e., a higher value of $P_{th}$) correlates with higher $n_{eff}$.

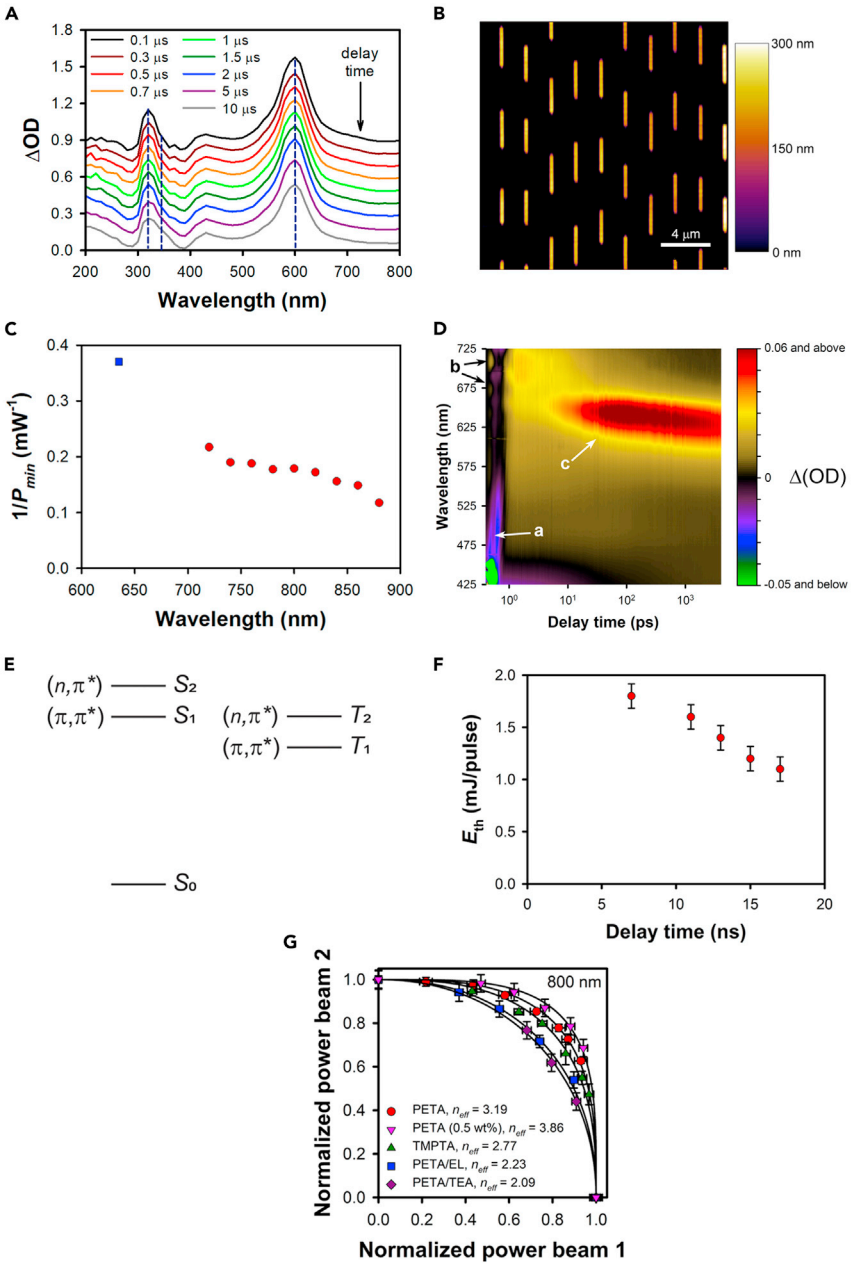


**Figure 2. Deactivation and self-deactivation of ITX**

(A) Transient-absorption spectra of ITX in ethylene glycol with 355 nm, 7 ns excitation pulses. The ΔOD scale is correct for the spectrum with a 10 μs delay. Each subsequent spectrum, moving from longer delays to shorter delays, has been offset by 0.1 units vertically from the previous one for clarity. The vertical dashed lines indicate spectral features that are discussed in the text.

(B) AFM images of lines written in an ITX/PETA photoresist with 800 nm, 150 fs laser pulses at a stage velocity of 20 μm/s. A chopped, spatially overlapped, 800 nm, CW beam was used to inhibit polymerization. The average excitation power was 5 mW and the deactivation power was 30 mW. The scale bar represents 4 μm.

(C) Deactivation action spectrum of the photoresist following excitation with 800 nm, 150 fs laser pulses at an average excitation power of 8.2 mW. The blue square is for deactivation with a 635 nm diode laser, and the red circles are for deactivation with a Ti:sapphire oscillator in CW mode.

(D) Ultrafast pump/probe spectrum of ITX in glyme. Excitation was performed at 400 nm, and white-light continuum was used as the probe. See text for an explanation of the labels (A–C).

(E) Representative Jablonski diagram for ITX in a polar solvent.

**Figure 2. *Continued***

(F) Delay-time dependence of the threshold pulse energy for deactivation at 630 nm of the ITX/PETA photoresist following excitation with 315 nm pulses. Both beams had a pulse duration of 7 ns and a repetition rate of 10 Hz. The error bars represent the estimated uncertainty in determining the deactivation threshold.

(G) 2-BIT data and the corresponding $n_{eff}$ values for photoresists based on PETA (circles, 1.5 wt% ITX, and down triangles, 0.5 wt% ITX), TMPTA (up triangles, 1.5 wt% ITX), PETA and ethyl lactate (squares, 1.5 wt% ITX), and PETA and triethylamine (diamonds, 1.5 wt% ITX).

The error bars in (F) and (G) represent $\pm 1$ standard deviation, as determined by making multiple measurements.

## Triplet-state absorption

A previous study suggested that stimulated emission is responsible for the strong inhibition dynamics that ITX/PETA photoresists exhibit under irradiation at 532 nm (Fischer et al., 2010). Subsequent ultrafast, pump-probe spectroscopy experiments revealed that at deactivation wavelengths longer than 500 nm, the influence of stimulated emission on deactivation is negligible (Wolf et al., 2011). Harke et al. studied the inhibition of ITX photoresists with a deactivation wavelength of 630 nm (Harke et al., 2013), and suggested that the long-lived photogenerated species in ITX are triplet states. It was therefore proposed that the inhibition mechanism in this photoresist involves depletion of the lowest triplet state ($T_1$) of ITX when the deactivation beam is resonant with transition between $T_1$ and a higher triplet state. Although triplet absorption followed by RISC from a highly excited triplet state to a high singlet state has been suggested to be the deactivation mechanism (Chi et al., 2019, 2021; Harke et al., 2013), no direct evidence has been provided for this process.

The triplet quantum yield of thioxanthones can be as high as 85% (Allonas et al., 2000; Amirzadeh and Schnabel, 1981), underscoring the potential importance of triplet-state dynamics in these systems. To investigate these dynamics, we studied ITX solutions using a transient absorption (TA) spectrometer with a temporal resolution of 0.1 μs. TA is a powerful means of studying excited triplet states and identifying short-lived intermediates (Kajii et al., 1991). The time evolution of the TA spectrum of ITX in ethylene glycol following excitation at 355 nm is shown in Figure 2A. There are two major features in the initial spectrum, one at ~318 nm and another at ~605 nm (see dashed vertical lines in Figure 2A). Each of these peaks is assigned to absorption from both $T_1$ and $T_2$ to higher triplet states of ITX, on the basis of earlier reports (Rai-Constapel et al., 2011). The initial peaks decay over a timescale that is considerably longer than the longest delay time studied, 10 μs. A new peak grows in at ~345 nm on a timescale of a few μs. We attribute this new feature to absorption of ketyl radicals that are created via H-atom transfer from the solvent to the carbonyl group of ITX in the $T_{2\ state}$. The fact that ketyl radicals can be formed on a timescale that is considerably longer than the expected lifetime of the $T_2$ state suggests that this state is at least somewhat thermally accessible from the $T_1$ state in ethylene glycol.

The triplet absorption features of ITX are generally long-lived, having lifetimes of tens of μs or longer, depending on the solvent (Table S1). Interestingly, the triplet absorption spectrum is non-zero at 800 nm, and can extend to 900 nm or beyond. This observation raises the question of whether ITX triplet states can be deactivated within this wavelength region. To investigate this scenario, we fabricated polymer lines in ITX photoresists using ultrafast excitation at 800 nm, while simultaneously irradiating with CW light at a wavelength of 800 nm. The two beams were spatially coincident, and the CW beam was chopped. As evidenced by the atomic force microscopy (AFM) data in Figure 2B, 800 nm radiation can indeed cause complete inhibition of polymerization. The fact that the same color of light used for excitation also promotes deactivation suggests that deactivation can be induced by the same laser pulse train that is used for excitation, decreasing the efficiency of the exposure. We term this phenomenon "self-deactivation."

Our results are consistent with the previous conjecture (Harke et al., 2013) that deactivation involves triplet absorption. However, a more rigorous test of this hypothesis requires a comparison of the wavelength dependences of triplet absorption and deactivation. To this end, we developed a technique that we call deactivation action spectroscopy (DAS). In the case of ITX-based photoresists, DAS was implemented by keeping the excitation conditions the same (i.e., wavelength, average power, and stage velocity), while varying the deactivation wavelength and power. At each deactivation wavelength, we determined the minimum CW laser power required to cause complete inhibition of polymerization. Assuming that deactivation occurs through linear absorption, the DAS spectrum is a plot of the inverse of the threshold power for deactivation as a function of deactivation wavelength. As shown in Figure 2C, DAS data in an ITX-based photoresist bear a strong resemblance to the triplet absorption spectrum in the same wavelength range

(Figure 2A). This correspondence provides additional evidence that triplet absorption is a key step in deactivation.

We performed ultrafast transient absorption spectroscopy on a solution of ITX in glyme to explore faster triplet dynamics. Figure 2D is a heatmap of the time-resolved absorbance change following ultrafast excitation at 400 nm. For ~500 fs after excitation there is a negative feature (labeled a) from ~400 nm to ~550 nm that arises from stimulated emission. A longer-lasting feature at the shorter end of this wavelength range arises from a ground-state bleach. After ~500 fs, two positive, excited-state absorption (ESA) features (labeled b) grow in at ~660 nm and ~700 nm. The Jablonski diagram in Figure 2E shows the energy levels of ITX in a typical polar organic solvent. The $S_1$ and $S_2$ states of ITX have similar energies, in analogy to what is known for the parent molecule thioxanthone (TX) (Villnow et al., 2014). One of these states has ($n$,$\pi^*$) character, whereas the other has ($\pi$,$\pi^*$) character. Density functional theory (DFT) calculations showed that the energetic ordering of the states depends on the nature of the solvent (Figures S4–S8). In THF and ethyl acetate, the ($n$,$\pi^*$) singlet state has the lower energy, whereas in water and ethylene glycol the ($\pi$,$\pi^*$) singlet state has the lower energy. Because glyme is a polar, aprotic solvent, we assign the ESA feature at ~660 nm to the ($n$,$\pi^*$) singlet state and the feature at ~700 nm to the ($\pi$,$\pi^*$) singlet state, assuming that ESA leads to the same higher excited state from $S_1$ and $S_2$. Although absorption from these states could potentially appear immediately following excitation, the ~500 fs lag time observed presumably arises from a combination of vibrational relaxation and the existence of a negative-going feature in the same spectral region, which can be seen most clearly at wavelengths longer than 700 nm.

At delay times between 1 ps and 10 ps, there is evidence in the ESA bands for population changes in the excited singlet states (Figure S9). The blue shift of the ESA bands over this same time period reflects solvation dynamics (Abdullah and Kemp, 1986). Within 20 ps, the ESA feature has decayed, and a positive feature has grown in at ~650 nm. This latter feature is the result of population growth in a triplet state via ISC. We therefore conclude that the time constant for the equilibration between the $S_1$ and $T_2$ states is on the order of 10–20 ps. The triplet absorption feature (labeled c) shifts to the blue on the nanosecond timescale. The triplet state initially populated is not the lowest triplet state, so this shift reflects a combination of equilibration between the triplet states and solvation. In the solvent in which these spectra were obtained, glyme, the ($\pi$,$\pi^*$) triplet state should have the lowest energy, with the ($n$,$\pi^*$) triplet being the state through which ISC occurs (Mundt et al., 2016; Villnow et al., 2014), again in analogy with TX (Rai-Constapel et al., 2014).

We developed an *in situ* technique to monitor exposure (i.e., crosslinking of a photoresist film) and deactivation to examine in more detail how triplet dynamics are manifested in a photoresist (Figure S10). Large-area exposures were performed at a repetition rate of 10 Hz and a wavelength of 315 nm using the frequency-doubled output of an optical parametric oscillator (OPO) with a pulse length of ~7 ns. The 630 nm fundamental of the OPO was used for deactivation. The minimum deactivation power for a fixed exposure time was determined as a function of the time delay between the 315 nm and 630 nm pulses. No deactivation was observed when the deactivation pulse preceded the excitation pulse. Figure 2F shows the deactivation threshold for delay times ranging from 7 ns to 17 ns, a range over which the threshold decreases by ~40%.

These results yield key insights into the photophysics of deactivation based on the increase in deactivation efficiency with increasing delay time. The ($n$,$\pi^*$) triplet state is expected to be reactive, but the TA experiments discussed above show that this state generates radicals on a timescale much longer than 17 ns. The 100 ms repetition time used for the large-area exposure experiments is sufficient to allow all excited molecules to relax between pulses, as is the case in the TA experiments described above. Thus, the excitation and deactivation in this experiment must occur on a shot-by-shot basis. Based on the data in Figure 2D, the ($n$,$\pi^*$) triplet state undergoes internal conversion to the ($\pi$,$\pi^*$) triplet state on a timescale of nanoseconds. This timescale is highly dependent on the solvent environment (Angulo et al., 2010; Villnow et al., 2014). It appears that relaxation to the ($\pi$,$\pi^*$) triplet state enhances the efficiency of deactivation. Because internal conversion and deactivation are both first-order in the concentration of the ($n$,$\pi^*$) states, the order in which these processes occur does not affect the ultimate ($n$,$\pi^*$) population. Thus, the ($\pi$,$\pi^*$) triplet state serves as a long-term, inert reservoir, but the ($n$,$\pi^*$) triplet state remains thermally accessible to population in the ($\pi$,$\pi^*$) state. Furthermore, deactivation occurs more efficiently from the ($\pi$,$\pi^*$) state than from the ($n$,$\pi^*$) state. This phenomenon is likely due to a larger transition dipole for ($\pi$,$\pi^*$) absorption to a higher triplet state. Together, these effects account for the data in Figure 2F.

We note that the details of exposure are different for excitation with a Ti:sapphire oscillator, as the oscillator repetition time is on the order of 13 ns, rather than 100 ms. With the short repetition time of the Ti:sapphire laser, the ($n,\pi^*$) triplet state is continuously replenished, so that initiation can occur even in a resist in which $T_2$ is not thermally accessible from $T_1$. We expect that the chemical nature of the monomers will have an influence on the exposure/deactivation behavior of an ITX-based photoresist. With this idea in mind, we performed 2-BIT experiments on additional ITX photoresists. We prepared a photoresist with trimethylolpropane triacrylate (TMPTA) as the monomer, and in another we added 20 wt% of ethyl lactate to the ITX/PETA mixture. As can be seen in Figure 2G, $n_{eff}$ drops from 3.19 $\pm$ 0.05 to 2.77 $\pm$ 0.05 in moving from the ITX/PETA photoresist to the ITX/TMPTA photoresist. The decrease in $n_{eff}$ results from chemical and/or physical differences that cause ITX/TMPTA to have a lower deactivation efficiency than ITX/PETA, resulting in less self-deactivation by the excitation beam.

The addition of the ethyl lactate to the ITX/PETA photoresist results in an even more dramatic reduction of $n_{eff}$, to 2.23 $\pm$ 0.05. We performed TA experiments on ITX solutions containing different percentages of ethyl lactate to delve into the cause of this behavior. These studies revealed that the triplet-state lifetime of ITX decreases with increasing ethyl lactate concentration, and that the signal from the ketyl radical appears rapidly in this solvent (Figure S11). These results indicate that ethyl lactate acts as a coinitiator, transferring a hydrogen atom to a molecule in the ($n,\pi^*$) triplet state much more rapidly than the monomers can.

We next made 2-BIT measurements in an ITX/PETA photoresist containing a common coinitiator, triethylamine, to confirm the influence of such species on $n_{eff}$. In this case $n_{eff}$ dropped even further, to 2.09 $\pm$ 0.05 (Figure 2G). The considerably more rapid reaction of the triplet-state molecules in the presence of a coinitiator renders self-deactivation less effective, because radical initiation can commence before relaxation to the lowest triplet state. The more efficient the coinitiator, the more rapid the initiation process, and the less effective the self-deactivation process.

An additional implication of the self-deactivation scenario is that the value of $n_{eff}$ will depend on the concentration of the photoinitiator. The lower the concentration of the photoinitiator, the higher the threshold intensity for polymerization. A higher threshold intensity leads to an increased amount of self-deactivation, which is predicted to cause $n_{eff}$ to increase. Indeed, we find that with 800 nm excitation, the $n_{eff}$ value of 3.19 $\pm$ 0.05 measured in a PETA photoresist with 1.5 wt% of ITX increases to 3.86 $\pm$ 0.05 when the photoinitiator concentration is decreased to 0.5 wt% (Figure 2G).

## Phosphorescence

Phosphorescence provides another means of investigating triplet photophysics. The luminescence intensity, including both fluorescence from $S_1$ and phosphorescence from $T_1$, has the advantage of being linear in the concentration of excited molecules, which is not the case for photopolymerization (Liaros and Fourkas, 2021; Yang et al., 2019). We developed a luminescence deactivation technique to probe the photophysics of deactivation. An ultrafast laser was used to excite an ITX solution through a high-numerical-aperture objective, and luminescence was collected epifluorescently. We chose PEG-400 as the solvent, because this material approximates the photoresist in polarity and viscosity. A second CW laser beam that could be tuned through in a wavelength range known to deactivate photoresists containing ITX (740 nm–840 nm) was focused through the same objective. The focal volumes of the two beams were overlapped in three dimensions.

As shown in Figure 3A, the CW beam had an inhibitory effect on the luminescence that exhibits the same qualitative wavelength dependence observed in the deactivation action spectrum in Figure 2C, in which shorter wavelengths provide more efficient deactivation. The decrease in the luminescence is linear in the deactivation power. To examine this phenomenon further, we used 800 nm deactivation and probed the luminescence in different spectral windows (Figure 3B). With unfiltered emission, for powers up to 50 mW, the deactivation is limited to a few percent. A 435 nm bandpass filter with a full width at half maximum bandwidth of 48 nm restricts transmission to the wavelength region of the ITX fluorescence spectrum (Figure S12), although some phosphorescence should fall within this window as well (Chi et al., 2021). When this filter is used, virtually no deactivation is observed (Figure 3B). A 550 nm longpass filter blocks the fluorescence of ITX, but transmits some of the phosphorescence (Chi et al., 2021). When this filter is used, substantial deactivation is observed (Figure 3B), which suggests that the small amount of deactivation

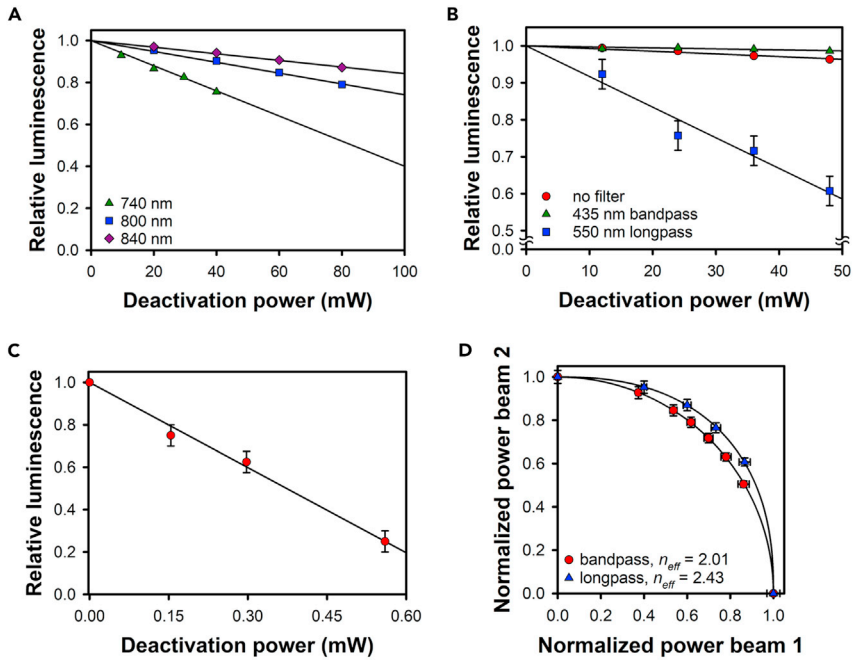


**Figure 3. Luminescence studies of ITX in PEG-400**

(A) Luminescence as a function of CW deactivation power. Excitation was performed using 800 nm, 150 fs pulses, and deactivation was performed at 740 (triangles), 800 nm (squares), and 840 nm (diamonds).

(B) Inhibition of luminescence by 800 nm light with detection in different spectral windows: unfiltered (circles), with a 445 nm bandpass filter to capture predominantly fluorescence (triangles), and with a 550 nm longpass filter to capture only phosphorescence (squares).

(C) Inhibition of luminescence by 635 nm light using a longpass filter with a 645 nm cutoff. Phosphorescence deactivation is extremely efficient at this wavelength.

(D) 2-BCEIn data for fluorescence (circles) and phosphorescence (triangles) with ultrafast, 800 nm excitation. The difference in $n_{eff}$ between the two datasets indicates that self-deactivation plays a role in the phosphorescence data. The error bars in all panels represent $\pm 1$ standard deviation, as determined by making multiple measurements.

observed with the 435 nm bandpass filter is also due to inhibition of phosphorescence. In all cases, the deactivation was linear in the power of the 800 nm CW laser.

The polymerization deactivation action spectrum (Figure 2C) indicates that deactivation is considerably more efficient at 635 nm than at 800 nm. We therefore tested the ability of CW, 635 nm light to deactivate phosphorescence, in this case using a 645 nm longpass filter so that scatter from the deactivation beam would not be detected. Using an efficient deactivation wavelength and filtering out all fluorescence facilitates the sensitive detection of phosphorescence deactivation. As shown in Figure 3C, this scheme enables extremely efficient phosphorescence deactivation of ITX, with a reduction of emission of greater than 80% at a laser power of less than 0.6 mW.

The luminescence observed using longpass filters serves as a proxy for the population of $T_1$, which is the ($\pi$,$\pi$*) triplet state in this solvent. Given that virtually no deactivation is observed when detection is restricted to the spectral window of the fluorescence spectrum, our results exclude stimulated emission as the mechanism of deactivation at the CW wavelengths studied here. The $T_2$ ($n$,$\pi$*) state is expected to have a shorter intrinsic phosphorescence lifetime than the $T_1$ ($\pi$,$\pi$*) state (Villnow et al., 2014). However, because the ($n$,$\pi$*) triplet has an energy similar to that of the first excited singlet state, phosphorescence from $T_2$ will occur in essentially the same wavelength range as fluorescence. In contrast, $T_1$ is the most stable triplet state, and so will phosphoresce at longer wavelengths than does $T_2$. With the 645 nm longpass filter, the only phosphorescence detected should therefore arise from $T_1$.

We next measured $n_{eff}$ independently for fluorescence and phosphorescence. For these measurements, we employed another technique that we have developed recently, 2-beam constant emission intensity

(2-BCEIn) spectroscopy (Liaros et al., 2018b). 2-BCEIn is analogous to 2-BIT, except that $n_{eff}$ is measured for the emission intensity (Figure S13). In contrast to traditional methods for studying emission induced by nonlinear absorption, 2-BCEIn can determine $n_{eff}$ at any given emission intensity, using only a limited range of average excitation powers.

We note that $n_{eff}$ in a given system is dependent on the observable. For 2-photon excitation of ITX, we expect that $n_{eff} = 2$ for fluorescence but that $n_{eff} > 2$ for phosphorescence, because self-deactivation will play a role in phosphorescence that is similar to its role in photopolymerization. 2-BCEIn measurements in ITX solutions using 800 nm ultrafast excitation bear out this prediction, as shown by the data in Figure 3D. When a 435 nm bandpass filter is used to probe fluorescence, the measured value of $n_{eff}$ is $2.01 \pm 0.05$. This value of $n_{eff}$ agrees with the results of previous studies using the Z-scan technique, in which ultrafast excitation was reported to take place via 2PA (Chi et al., 2021). However, when the phosphorescence is probed by using a longpass filter, we find that $n_{eff} = 2.42 \pm 0.05$. The measured exponents were independent of whether the beams were spatially overlapped, indicating that the 2-BCEIn data were not affected by repetition-rate-dependent effects.

These results place strong constraints on the deactivation mechanism of ITX. It has been suggested previously that deactivation involves excitation to a higher triplet state that then undergoes RISC to an excited singlet state (Harke et al., 2013), which would presumably be higher in energy than $S_2$. The typical fate of such a state is to relax quickly to $S_1$ (Kasha, 1950). In this case, we expect that luminescence deactivation experiments would show a decrease in phosphorescence, accompanied by an increase in fluorescence, due to repopulation of $S_1$. Given the high triplet quantum yield for $S_1$ in ITX, this mechanism would also repopulate $T_1$ and $T_2$, and so deactivation would not be efficient. A second, less common fate of high singlet states is to undergo ISC to the triplet manifold. This process would also repopulate $T_1$ and $T_2$ through rapid internal conversion, and so is not an efficient path for deactivation.

Radiationless relaxation in the singlet manifold is another possible deactivation mechanism (Fischer et al., 2013). This process could occur in two different manners. The first is that higher excited singlet states undergo internal conversion directly to the ground electronic state. This scenario is unlikely, but not impossible (Villnow et al., 2014). The more plausible explanation is that a higher triplet state undergoes RISC directly to a highly vibrationally excited level of the ground electronic state, a process that is known to occur in other aromatic molecules (Callomon et al., 1972; Knee and Johnson, 1985; Otis et al., 1983). The high density of states of $S_0$ at the energy of a higher triplet state is favorable for RISC from the perspective of Fermi's golden rule. This mechanism could lead to a small increase in fluorescence in the luminescence deactivation experiments, due to repopulation of the ground state, but this increase would be counterbalanced by the inhibition of phosphorescence in the same wavelength region. Furthermore, in photoresists, a mechanism that regenerates the ground electronic state is the only plausible scenario in which efficient deactivation could occur.

## Kinetic modeling

To assess the viability of the proposed self-deactivation mechanism further, we next present a simple kinetic model. Our model contains two electronic states, the ground singlet $S_0$ and the lowest triplet $T_1$, as shown in Figure 4A. ISC to $T_1$ is assumed to take place instantaneously upon 2PA, the latter of which occurs with rate constant $k_2 I^2$, where $I$ is the irradiance. Because ISC is assumed to be instantaneous, the state $S_1$ is not included explicitly in the model, although the branching ratio for ISC is included implicitly in $k_2$. RISC to $S_0$ is assumed to take place instantaneously following linear absorption from $T_1$, the latter of which occurs with rate constant $k_1 I$. The higher triplet state through which RISC occurs is not included explicitly in the model, and the branching ratio for RISC is included implicitly in $k_1$. Intramolecular vibrational relaxation (IVR) is assumed to be instantaneous in the ground electronic state.

The derivation of the kinetic equations is given in the STAR methods. The goal of the kinetic model is to determine how $n_{eff}$ depends on $k_1$ and $k_2$. We model a train of square pulses at repetition rate $f$, such that the duty cycle $D$ is the pulse duration multiplied by $f$. The key result is that the fraction of population in the triplet state following an exposure of duration $t'$ is given by

$$\frac{[T_1]_{t'}}{[S_0]_0} = \frac{\frac{k_2 I^2}{D}}{k_1 I + \frac{k_2 I^2}{D}} \left(1 - \exp\left[-\left(k_1 I + \frac{k_2 I^2}{D}\right) t'\right]\right). \qquad \text{(Equation 2)}$$

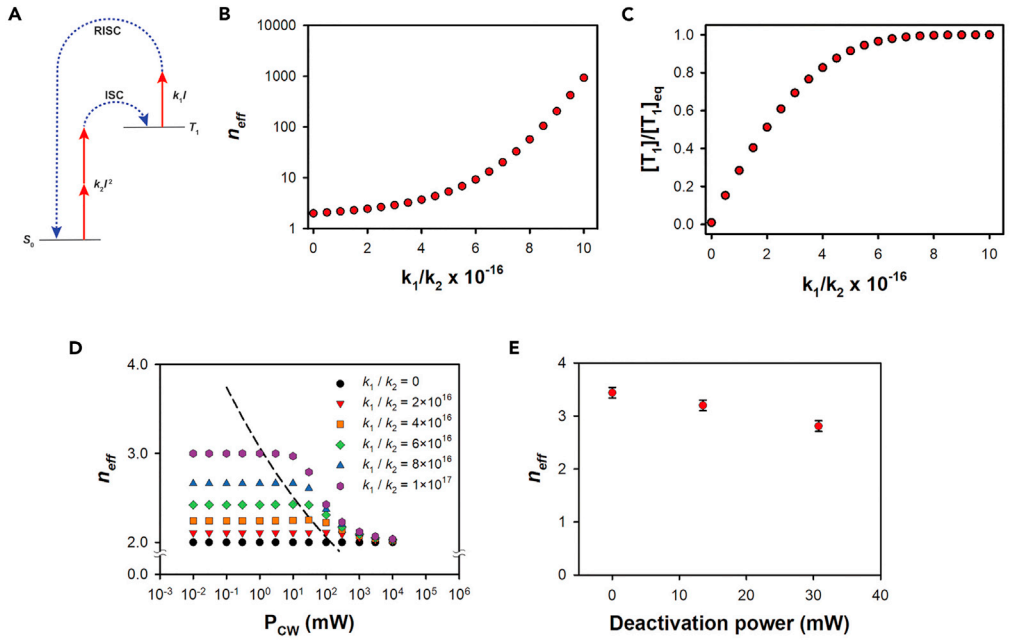


**Figure 4. Kinetic model for self-deactivation**

(A) Schematic of a kinetic model that incorporates 2-photon excitation with rate constant $k_2 I^2$ and linear deactivation with rate constant $k_1 I$, where $I$ is the irradiance.

(B) Dependence of $n_{eff}$ on $k_1/k_2$ (in units of kg/s$^3$) for parameters given in the text.

(C) Ratio of the triplet population to the equilibrium triplet population as a function of $k_1/k_2$ for the same parameters as in (B).

(D) Dependence of $n_{eff}$ on the power of a CW deactivation beam for different values of $k_1/k_2$ for the same parameters as in (B). The dashed line indicates the positions of the maxima in the curves.

(E) Value of $n_{eff}$ as a function of deactivation power in 2-BITD experiments on the ITX/PETA photoresist. The error bars represent $\pm$1 standard deviation, as determined by making multiple measurements.

Here, we assume that the polymerization threshold is reached when 1% of the population is in the triplet state (i.e. $[T_1]_{t'}/[S_0]_0 > 0.01$). The qualitative conclusions from this treatment do not depend on the value of the threshold.

The measurement of $n_{eff}$ using 2-BIT relies on the concept of limited reciprocity, which means that if the exposure time is kept constant, then the same degree of crosslinking will occur regardless of the details of how the exposure is distributed within the exposure window (Liaros and Fourkas, 2021). 2-BIT experiments are performed at a single repetition rate, but the same exponent can be obtained by determining the threshold irradiance for polymerization as a function of the repetition rate (Fischer and Wegener, 2013; Liaros and Fourkas, 2021). When the repetition rate is varied in a system exhibiting limited reciprocity, the peak pulse irradiance $I_{p,th}$ obeys the relation

$$I_{p,th} \propto f^{1/n_{eff}}. \qquad \text{(Equation 3)}$$

Thus,

$$n_{eff} = -\frac{d\ln(f)}{d\ln(I_{p,th})}. \qquad \text{(Equation 4)}$$

Here, we start by choosing a base repetition rate $f$ and then determining $I_{p,th}$ at $f$, 0.99$f$, and 1.01$f$. We determine $n_{eff}$ by averaging the values calculated from Equation 4 with 0.99$f$ and $f$ and with $f$ and 1.01$f$. We used $f$ = 80 MHz and a pulse length of 200 fs. The radius of the laser spot size was chosen to be 0.5 μm and the exposure time 0.025 s (corresponding to a scanning speed of ~40 μm/s). The value of $k_2$ was held constant at 2.21 × $10^{-25}$ s$^5$/kg$^2$, and $k_1$ was varied.

Figure 4B shows a plot $n_{eff}$ as a function of the value of $k_1$. As expected, $n_{eff}$ = 2 when $k_1$ = 0. As $k_1/k_2$ increases over an order of magnitude from $10^{-16}$ to $10^{-15}$ kg/s$^3$, $n_{eff}$ increases by a factor of nearly 1000.

This result illustrates that self-deactivation has a strong effect on the measured exponent, and that $n_{eff}$ alone is not a reliable indicator of the actual number of photons involved in the absorption process in molecules that are subject to this phenomenon.

The equilibrium (maximum) fractional population of the triplet state in Equation 2 is found by setting $t' = \infty$:

$$\frac{[T_1]_{eq}}{[S_0]_0} = \frac{\frac{k_2 I^2}{D}}{k_1 I + \frac{k_2 I^2}{D}}. \quad \text{(Equation 5)}$$

At any time $t'$, the fraction of the population in $T_1$ relative to its maximum value is given by

$$\frac{[T_1]_{t'}}{[T_1]_{eq}} = \left(1 - \exp\left[-\left(\frac{k_2 I^2}{D} + k_1 I\right) t'\right]\right). \quad \text{(Equation 6)}$$

As shown in Figure 4C, Equation 6 indicates that as $k_1$ grows larger, $[T_1]_{t'}$ approaches $[T_1]_{eq}$ asymptotically. Once the concentration of $T_1$ is near its maximum value, $I_{p,th}$ is insensitive to changes in $k_1$, based on Equation 3. Accordingly, $I_{p,th}$ changes less with repetition rate, leading to an increased value of $n_{eff}$. Indeed, as we show in the STAR methods, when $[T_1]_{t'} = [T_1]_{eq}$, $n_{eff}$ becomes infinite.

The qualitative behavior observed in this kinetic model is consistent with our experimental observations, pointing to self-deactivation as the cause of the large measured values of $n_{eff}$. As shown in Figures 1D and 1E, with increasing fabrication wavelength in the range explored here, $k_1$ decreases gradually and $k_2$ decreases rapidly. Therefore, $k_1/k_2$ increases with wavelength, causing a corresponding increase in $n_{eff}$.

We used the kinetic model to make an experimentally testable prediction regarding what happens if $n_{eff}$ is measured in the presence of a CW deactivation beam. In this case, the equation for the fraction of population in $T_1$ becomes

$$\frac{[T_1]_{t'}}{[S_0]_0} = \frac{\frac{k_2 I^2}{D}}{k_1 (I + I_d) + \frac{k_2 I^2}{D}} \left(1 - \exp\left[-\left(k_1 (I + I_d) + \frac{k_2 I^2}{D}\right) t'\right]\right), \quad \text{(Equation 7)}$$

where $I_d$ is the irradiance of the deactivation beam. The behavior of $n_{eff}$ as a function of the deactivation power is shown in Figure 4D for different values of $k_1/k_2$; in this case, the value of $k_2$ was reduced to $2.21 \times 10^{-26}$ $s^5/kg^2$, an order of magnitude lower than the value used above. The value of $n_{eff}$ is nearly constant at low deactivation powers, but does reach a maximum at the CW deactivation power values denoted by the dashed line in Figure 4D. In this range of deactivation powers, the increase in the threshold irradiance causes the excitation beam to promote even greater self-deactivation. At higher deactivation powers, $n_{eff}$ drops, eventually reaching a value of 2. When the deactivation power is higher than the excitation power, the deactivation beam is the major source of deactivation. The smaller the fraction of the deactivation that comes from the excitation beam, the closer $n_{eff}$ gets to 2.

We developed a class of techniques called 2-beam action with deactivation (2-BAD) spectroscopies to test the prediction of our model (Figure S14). In this case, we performed 2-BIT in the presence of a CW deactivation beam, in a method we call 2-beam initiation threshold with deactivation spectroscopy (2-BITD). In Figure 4E, we show that, in agreement with the predictions of our model, $n_{eff}$ decreases with increasing deactivation power. In these experiments, the ITX/PETA photoresist was exposed with pulsed 800 nm light and deactivated with CW 800 nm light.

## Implications for resolution

In principle, a higher order of absorption is desirable in MAP, providing improved resolution due to the greater degree of spatial confinement of the optical exposure. However, this notion is based upon $n_{eff}$ being a measure of the actual number of photons involved in exciting the photoinitiator from $S_0$ to $S_1$. The results presented above demonstrate that for ITX, $n_{eff}$ does not reflect the total number of photons that are involved in this transition, but rather can be thought of as the effective number of photons needed on average to yield a photoinitiation event. In light of this interpretation of the meaning of $n_{eff}$, it is important to examine whether a higher $n_{eff}$ translates into better resolution in ITX-based photoresists.

We used the kinetic model developed above to determine the spatial distribution of triplets in the focal plane for values of $n_{eff}$ ranging from 2.0 to 4.5 (roughly the range seen in the 2-BIT data presented here). We assume a

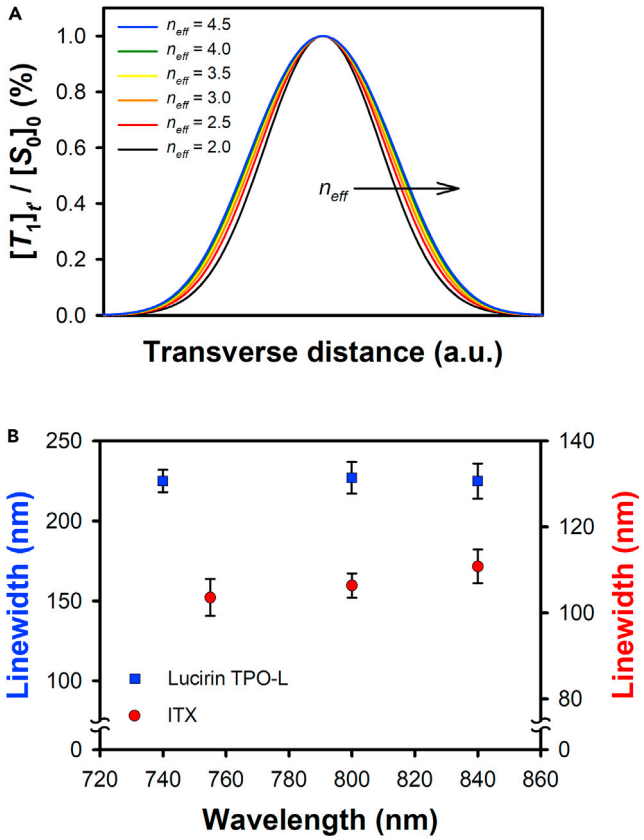


**Figure 5. Relationship between feature size and $n_{eff}$ in an ITX/PETA photoresist**

(A) Spatial dependence of the fractional triplet population in the kinetic model for different values of $n_{eff}$ at the peak intensity. The spatial intensity distribution was assumed to be Gaussian, and $k_2$ was fixed at 2.21 × $10^{-26}$ $s^5/kg^2$.

(B) Minimum experimental linewidth as a function of excitation wavelength for the ITX/PETA photoresist (red, right axis) and a control photoresist with Lucirin TPO-L as the photoinitiator (blue, left axis). These data demonstrate that a higher $n_{eff}$ in the ITX photoresist correlates with a broader linewidth. The error bars represent ±1 standard deviation, as determined by making multiple measurements.

Gaussian distribution of irradiance transverse to the direction of laser propagation, use $k_2$ = 2.21 × $10^{-26}$ $s^5/kg^2$, and for each $n_{eff}$ find the value of $k_1$ such that the peak value of $[T_1]_t/[S_0]_0$ is 0.01. The results of this modeling are shown in Figure 5A. We find that as $n_{eff}$ increases, the spatial distribution of triplet states becomes broader rather than narrowing. This behavior arises from the fact that the self-deactivation is strongest where the irradiance is the highest, i.e., in the center of the beam, thus flattening out the top of the peak of the triplet distribution. Thus, when $n_{eff}$ is larger than the number of photons involved in the transition from $S_0$ to $S_1$, we predict that the effect of increasing $n_{eff}$ is to degrade, rather than enhance, the spatial resolution.

We tested these predictions experimentally by creating sets of polymerized lines using different excitation wavelengths. For each wavelength, lines were fabricated at a range of different irradiances. Scanning electron microscopy was used to determine the width of the narrowest lines that survived development. The measured average linewidths are plotted as a function of excitation wavelength in Figure 5B. If absorption from $S_0$ to $S_1$ is a 2-photon process and there is no deactivation, then $n_{eff}$ = 2. In this case, the longest wavelength would yield the broadest lines, with the linewidth being proportional to the excitation wavelength. As shown in Figure 5B, experiments with such a photoinitiator, Lucirin TPO-L (Baldacchini et al., 2004), gave minimum linewidths that were effectively independent of excitation wavelength over the range from 740 nm to 840 nm. In ITX, if $n_{eff}$ represented the average number of photons absorbed to undergo a transition from $S_0$ to a higher singlet state, then based on the data in Figure 2D, the smallest feature size should be observed at the longest wavelength. However, as shown in Figure 5B, the linewidth in the ITX photoresist increases with increasing wavelength. This result agrees with the predictions of our model, and is indicative of the presence of self-deactivation.

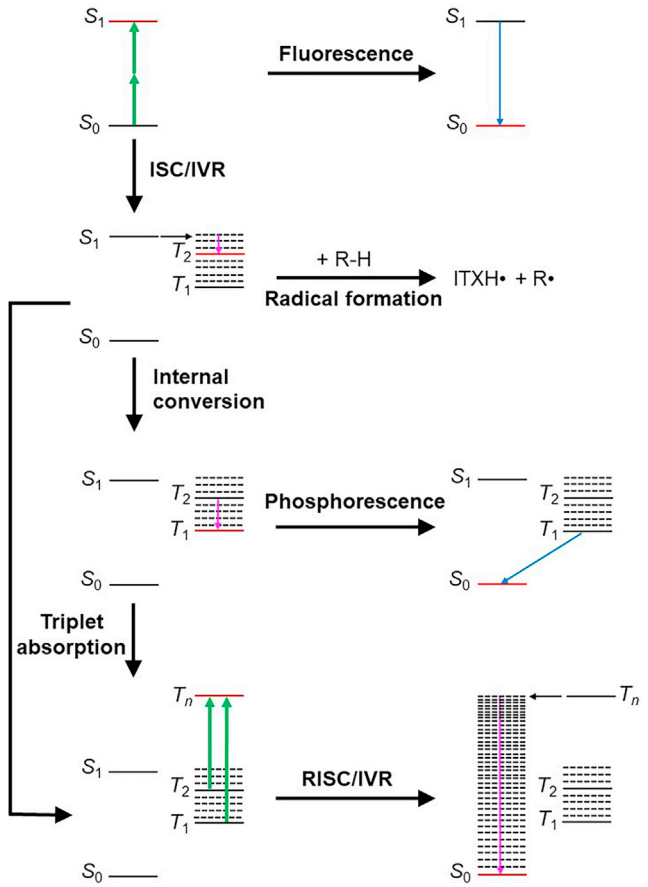


**Figure 6. Schematic representation of the most important photophysical processes that take place in the ITX photoresist, with the relevant states ($S_0$, $S_1$, $T_1$, $T_2$, and $T_n$) that are involved**

Green arrows indicate absorption of a photon, pink arrows indicate non-radiative relaxation, and blue arrows indicate radiative relaxation. Solid horizontal lines indicate vibrationless electronic states and dashed horizontal lines indicate vibrationally excited electronic states. The energy levels are not to scale. For each process, the final state is marked in red.

## DISCUSSION

The key photophysical steps in photopolymerization using ITX without a coinitiator are summarized in Figure 6. 2-photon excitation drives a transition between $S_0$ and $S_1$ and/or $S_2$ (the latter of which is not shown). Following excitation, the molecule can either fluoresce or undergo ISC to $T_2$ or a vibrationally excited level of $T_1$ (the latter case is not shown), in either case followed by IVR on a timescale of picoseconds. Molecules in the $T_2$ state can react with easily abstractable hydrogen atoms in the monomers. However, internal conversion from $T_2$ to $T_1$, the latter of which is unreactive, occurs on a timescale of nanoseconds. The $T_1$ state can phosphoresce or, depending on the energy gap between $T_1$ and $T_2$, which depends on the solvent, may be able to repopulate $T_2$ thermally (not shown). Irradiation at a wavelength that can cause deactivation takes population in either $T_1$ or $T_2$ to a higher triplet state that undergoes RISC rapidly to a highly vibrationally excited level of $S_0$, which relaxes on a picosecond timescale via IVR.

ITX is a complex model system, due to the nearly degenerate, and solvent-dependent energies of its lowest two singlet excited states and lowest two triplet states. The combination of techniques employed here enabled us to identify the initial triplet states involved in the optical deactivation of ITX, and also to ascertain the manner in which the singlet manifold is involved in the deactivation process. This pathway could not have been established unambiguously from any individual previously established technique or combination of such techniques. Furthermore, the knowledge that has been gained from our experiments and modeling provides clear guidance for the development of new TX derivatives with improved performance for 2CL. For instance, TX derivatives with an increased energy gap between the lowest two triplet

states and the next highest triplet states may not exhibit self-deactivation, which could lead to improved resolution.

The new spectroscopic toolkit presented here is broadly applicable to chemical systems that involve triplet photochemistry and photophysics. Our work demonstrates that 2-beam action spectroscopies enable the direct probing of triplet-state dynamics, and underscores the prospects for these methods to elucidate the mechanisms of complex triplet processes. The information obtained in the current study can be used to inform the synthesis of improved thioxanthone photoinitiators, but there are many other potential applications of 2-BA spectroscopies in areas of current interest in triplet dynamics. For instance, in the case of triplet–triplet annihilation upconversion (Bharmoria et al., 2020), 2-beam constant emission intensity spectroscopy offers a new approach to making precise measurements of the effective order of absorption at any given irradiance, providing a more sensitive means of determining when the linear excitation regime has been attained (Jacopo and Angelo, 2017).

The new spectroscopies presented here offer a clear path to characterizing and quantifying photodeactivation of triplets. If there is an observable that allows the triplet population to be determined (e.g., phosphorescence or photochemistry), then deactivation action spectroscopy can be used to determine the wavelength-dependent efficiency of deactivation. Wavelength-dependent 2-BA spectroscopies allow for the detailed probing of photochemistry and photophysics, and to identify and quantify any contributions from self-deactivation. These techniques can be used with whatever observables are available from the system of interest (e.g., fluorescence, phosphorescence, photochemistry, or photocurrent), and comparing the results for different observables and/or conditions can give valuable information about triplet photodeactivation. The ability to extract a precise exponent at a given value of an observable provides key advantages over traditional methods of measuring optical nonlinearity. Although we used 2-BA spectroscopies here to study processes involving multiphoton absorption, which requires a pulsed laser, if the observable is not a cumulative one (i.e., fluorescence and phosphorescence, but not photochemistry), then there is no requirement that the two beams be spatially overlapped. In this case, the beams can be CW rather than pulsed.

The addition of a separate deactivation beam in 2-BA spectroscopies adds another dimension to the ability to elucidate triplet dynamics. In MAP using an ITX-based photoresist, this extra beam decreased the apparent order of nonlinearity in the system. However, the effect of the extra beam on the observed exponent is dependent on the mechanism by which triplet photodeactivation occurs. 2-BAD spectroscopies therefore have the potential to provide additional mechanistic understanding in processes in which triplet photodeactivation is involved.

The ability to elucidate pathways for the photodeactivation of triplet states will make it possible to develop new materials with improved performance for many applications. For instance, in the case of organic LEDs, triplet states are a bottleneck, because these states are electrogenerated statistically three times as often as the desired, emissive singlet states (Baldo et al., 2000). A common approach to solving this problem is to engineer the energies of the electronic states to promote thermal RISC from the lowest triplet state (Yang et al., 2017). However, this approach increases the effective emission lifetime of molecules, slowing the cycling of their excitation. Incorporating efficient triplet photodeactivation is another potential path toward moving population from the triplet manifold into the singlet manifold. In other applications, such as photon upconversion via triplet–triplet annihilation (Bharmoria et al., 2020), photodeactivation of triplet states is a deleterious process. It is important to be able to characterize photodeactivation in such cases, so that systems can be designed that minimize this phenomenon.

Self deactivation of triplet states is a special case of photodeactivation that is not commonly considered in photochemistry and photophysics. Self-deactivation may be particularly important when multiphoton excitation is employed, as the irradiances used are much higher than for linear excitation, and so even a deactivation process that involves weak linear absorption can have a substantial effect. Our work here shows that self-deactivation can have a negative impact on the resolution in MAP, and the same may hold true for some other applications of multiphoton absorption, such as in 4-photon upconversion (Izakura et al., 2018). The characterization of the deactivation process is a key step toward developing molecules and/or choosing excitation wavelengths that minimize self-deactivation.

There are other applications in which self-deactivation is a desirable process. For example, in multiphoton fluorescence microscopy, triplet states can act as long-lived bottlenecks that reduce the fluorescence yield

and increase the probability of irreversible photobleaching (Donnert et al., 2007). Furthermore, for fluorophores with high symmetry, the triplet yield under multiphoton excitation can be higher than that for linear excitation, because a different excited state is accessed initially; consequently, the fluorescence quantum yield is decreased under multiphoton excitation (Liaros and Fourkas, 2017). Designing self-deactivation into fluorophores for multiphoton microscopy has the potential to break the triplet bottleneck, leading to more efficient emission.

## Conclusion

We have developed a suite of optical techniques for studying triplet-state dynamics. In combination with established spectroscopic methods, these techniques make possible the identification of the states and pathways involved in complex photophysical and photochemical phenomena involving triplet states. To demonstrate the power and versatility of this expanded toolkit, we applied these techniques to study the triplet-state dynamics of ITX that are involved in the use of this material as a photoinitiator in MAP and 2-color lithography.

The studies presented here highlight the advantages of using multiphoton absorption to study triplet dynamics. The differences in selection rules for linear and 2PA for highly symmetric molecules can provide access to different excited states, which in turn can lead to differences in triplet yields. More importantly, in less symmetric molecules, one of the main advantages of multiphoton, as opposed to linear, absorption lies in the differences in triplet absorption at the excitation wavelength. In the case of linear excitation, any triplet absorption will take the molecules to a highly excited triplet state that is more likely to be reactive than are lower triplet states. On the other hand, when multiphoton absorption is used for the initial excitation, triplet absorption can involve excitation to lower-lying triplet excited states that are less reactive and more likely to lead to deactivation.

The self-deactivation process described here is likely a common phenomenon in triplet-state dynamics, particularly when multiphoton absorption is employed. As was demonstrated above, self-deactivation not only plays a role in the polymerization kinetics of ITX-based photoresists, but also in the phosphorescence of this molecule in solution. Deactivation and self-deactivation are likely to be key elements for exerting new forms of control in many processes that involve triplet-state dynamics.

## Limitations of the study

The methods developed here are best suited to systems in which the yield of photogenerated triplet states is substantial. However, this requirement could in principle be circumvented by the use of an appropriate triplet sensitizer.

## STAR★METHODS

Detailed methods are provided in the online version of this paper and include the following:

- KEY RESOURCES TABLE
- RESOURCE AVAILABILITY
  - Lead contact
  - Materials availability
  - Data and code availability
- METHOD DETAILS
  - Substrate functionalization
  - Photoresist preparation
  - 2-BIT measurements
  - 2-BCEIn measurements
  - 2-color luminescence excitation/deactivation measurements
  - *In situ* measurements of polymerization and deactivation
  - Microsecond transient absorption
  - Ultrafast pump-probe spectroscopy
  - Density functional theory calculations
  - Details of the kinetic model

## SUPPLEMENTAL INFORMATION

Supplemental information can be found online at https://doi.org/10.1016/j.isci.2021.103600.

## ACKNOWLEDGMENTS

This work was supported by National Science Foundation, grants CMMI-1449309 and CHE-1800491. NL acknowledges support by the Research Corporation for Science Advancement (RCSA) and the National Science Foundation through a Cottrell Fellowship. The Cottrell Fellowship Initiative is partially funded by a National Science Foundation award to RCSA (CHE-2039044).

## AUTHOR CONTRIBUTIONS

N.L. and J.T.F. conceived the project. N.L. implemented and performed the 2-BA and multiphoton luminescence deactivation experiments and analyzed the data. S.G.R. prepared the samples for these measurements. N.L and S.G.R. performed the multiphoton absorption polymerization experiments and characterized their results using SEM measurements. J.T.F. supervised this portion of the research. H.M.O. performed the in-situ monitoring of exposure and deactivation experiments; A.S.M. supervised this portion of the research. M.D.T., A.N.Z., and S.W. performed the microsecond transient spectroscopy and DFT calculations; D.E.F. supervised this portion of the research. T.M. and M.J.K. performed the ultrafast transient spectroscopy measurements. J.T.F. performed the kinetic modeling. J.S.P. provided expertise and feedback. N. L. and J.T.F. drafted the manuscript. All authors discussed the results and edited the manuscript. J.T.F. supervised the project.

## DECLARATION OF INTERESTS

The authors declare no competing interests.

Received: October 1, 2021
Revised: November 10, 2021
Accepted: December 3, 2021
Published: January 21, 2022

## REFERENCES

Abdullah, K.A., and Kemp, T.J. (1986). Solvatochromic effects in the fluorescence and triplet—triplet absorption spectra of xanthone, thioxanthone and N-methylacridone. J. Photochem. *32*, 49–57. https://doi.org/10.1016/0047-2670(86)85006-7.

Allonas, X., Ley, C., Bibaut, C., Jacques, P., and Fouassier, J.P. (2000). Investigation of the triplet quantum yield of thioxanthone by time-resolved thermal lens spectroscopy: solvent and population lens effects. Chem. Phys. Lett. *322*, 483–490. https://doi.org/10.1016/s0009-2614(00)00462-0.

Amirzadeh, G., and Schnabel, W. (1981). On the photoinitiation of free radical polymerization-laser flash photolysis investigations on thioxanthone derivatives. Macromol.Chem. Phys. *182*, 2821–2835. https://doi.org/10.1002/macp.1981.021821027.

Andrzejewska, E., Zych-Tomkowiak, D., Andrzejewski, M., Hug, G.L., and Marciniak, B. (2006). Heteroaromatic thiols as co-initiators for type II photoinitiating systems based on camphorquinone and isopropylthioxanthone. Macromolecules *39*, 3777–3785. https://doi.org/10.1021/ma060240k.

Angulo, G., Grilj, J., Vauthey, E., Serrano-Andres, L., Rubio-Pons, O., and Jacques, P. (2010). Ultrafast decay of the excited singlet states of thioxanthone by internal conversion and intersystem crossing. ChemPhysChem *11*, 480–488. https://doi.org/10.1002/cphc.200900654.

Baldacchini, T., LaFratta, C.N., Farrer, R.A., Teich, M.C., Saleh, B.E.A., Naughton, M.J., and Fourkas, J.T. (2004). Acrylic-based resin with favorable properties for three-dimensional two-photon polymerization. J. Appl. Phys. *95*, 6072–6076. https://doi.org/10.1063/1.1728296.

Baldo, M.A., Adachi, C., and Forrest, S.R. (2000). Transient analysis of organic electrophosphorescence. II. Transient analysis of triplet-triplet annihilation. Phys. Rev. B *62*, 10967–10977. https://doi.org/10.1103/PhysRevB.62.10967.

Bharmoria, P., Bildirir, H., and Moth-Poulsen, K. (2020). Triplet–triplet annihilation based near infrared to visible molecular photon upconversion. Chem. Soc. Rev. *49*, 6529–6554. https://doi.org/10.1039/D0CS00257G.

Bretschneider, S., Eggeling, C., and Hell, S.W. (2007). Breaking the diffraction barrier in fluorescence microscopy by optical shelving. Phys. Rev. Lett. *98*, 218103. https://doi.org/10.1103/PhysRevLett.98.218103.

Buck, J.T., Boudreau, A.M., DeCarmine, A., Wilson, R.W., Hampsey, J., and Mani, T. (2019). Spin-allowed transitions control the formation of triplet excited states in orthogonal donor-acceptor dyads. Chem *5*, 138–155. https://doi.org/10.1016/j.chempr.2018.10.001.

Callomon, J.H., Parkin, J.E., and Lopez-Delgado, R. (1972). Non-radiative relaxation of the excited $\tilde{A}\ ^1B_{2u}$ state of benzene. Chem. Phys. Lett. *13*, 125–131. https://doi.org/10.1016/0009-2614(72)80059-9.

Carmichael, I., and Hug, G.L. (1986). Triplet–triplet absorption spectra of organic molecules in condensed phases. J. Phys. Chem. Ref. Data *15*, 1–250. https://doi.org/10.1063/1.555770.

Chang, Y.-L., Song, Y., Wang, Z., Helander, M.G., Qiu, J., Chai, L., Liu, Z., Scholes, G.D., and Lu, Z. (2013). Highly efficient warm white organic light-emitting diodes by triplet exciton conversion. Adv. Funct. Mater. *23*, 705–712. https://doi.org/10.1002/adfm.201201858.

Chi, T., Somers, P., Wilcox, D.A., Schuman, A.J., Iyer, V., Le, R., Gengler, J., Ferdinandus, M., Liebig, C., Pan, L., et al. (2019). Tailored thioxanthone-based photoinitiators for two-photon-controllable polymerization and nanolithographic printing. J. Polym. Sci. B Polym. Phys. *57*, 1462–1475. https://doi.org/10.1002/polb.24891.

Chi, T., Somers, P., Wilcox, D.A., Schuman, A.J., Johnson, J.E., Liang, Z., Pan, L., Xu, X., and Boudouris, B.W. (2021). Substituted thioxanthone-based photoinitiators for efficient

two-photon direct laser writing polymerization with two-color resolution. ACS Appl. Polym. *3*, 1426–1435. https://doi.org/10.1021/acsapm.0c01291.

Cohen, S.R., and Fourkas, J.T. (2019). Extracting information on linear and nonlinear absorption from two-beam action spectroscopy data. J. Phys. Chem. A *123*, 7314–7322. https://doi.org/10.1021/acs.jpca.9b06068.

Donnert, G., Eggeling, C., and Hell, S.W. (2007). Major signal increase in fluorescence microscopy through dark-state relaxation. Nat. Methods *4*, 81–86. https://doi.org/10.1038/nmeth986.

Evans, D.F., and Thompson, H.W. (1960). The effect of environment on singlet-triplet transitions of organic molecules. Proc. R. Soc. Math. Phys. Eng. Sci. *255*, 55–63. https://doi.org/10.1098/rspa.1960.0049.

Farrer, R.A., Butterfield, F.L., Chen, V.W., and Fourkas, J.T. (2005). Highly efficient multiphoton-absorption-induced luminescence from gold nanoparticles. Nano Lett. *5*, 1139–1142. https://doi.org/10.1021/nl050687r.

Farsari, M., and Chichkov, B.N. (2009). Two-photon fabrication. Nat. Photonics *3*, 450–452. https://doi.org/10.1038/nphoton.2009.131.

Fischer, J., Mueller, J.B., Kaschke, J., Wolf, T.J.A., Unterreiner, A.-N., and Wegener, M. (2013). Three-dimensional multi-photon direct laser writing with variable repetition rate. Opt. Express *21*, 26244–26260. https://doi.org/10.1364/OE.21.026244.

Fischer, J., Mueller, J.B., Quick, A.S., Kaschke, J., Barner-Kowollik, C., and Wegener, M. (2015). Exploring the mechanisms in STED-enhanced direct laser writing. Adv. Opt. Mater. *3*, 221–232. https://doi.org/10.1002/adom.201400413.

Fischer, J., von Freymann, G., and Wegener, M. (2010). The materials challenge in diffraction-unlimited direct-laser-writing optical lithography. Adv. Mater. *22*, 3578–3582. https://doi.org/10.1002/adma.201000892.

Fischer, J., and Wegener, M. (2011). Three-dimensional direct laser writing inspired by stimulated-emission-depletion microscopy [invited]. Opt. Mater. Express *1*, 614–624. https://doi.org/10.1364/OME.1.000614.

Fischer, J., and Wegener, M. (2013). Three-dimensional optical laser lithography beyond the diffraction limit. Laser Photonics Rev. *7*, 22–44. https://doi.org/10.1002/lpor.201100046.

Fourkas, J.T. (2016a). Fundamentals of two-photon fabrication. In Three-Dimensional Microfabrication Using Two-Photon Polymerization, T. Baldacchini, ed. (Elsevier), pp. 45–61. https://doi.org/10.1016/B978-0-323-35321-2.00003-0.

Fourkas, J.T. (2016b). STED-inspired approaches to resolution enhancement. In Multiphoton Lithography: Techniques, Materials, and Applications, R.L. Jürgen Stampfl and A. Ovsianikov, eds. (Wiley-VCH), pp. 111–128.

Fourkas, J.T., and Petersen, J.S. (2014). 2-Colour photolithography. Phys. Chem. Chem. Phys. *16*, 8731–8750. https://doi.org/10.1039/C3CP52957F.

Frisch, M.J., Trucks, G.W., Schlegel, H.B., Scuseria, G.E., Robb, M.A., Cheeseman, J.R., Scalmani, G., Barone, V., Mennucci, B., Petersson, G.A., et al. (2009). Gaussian 09, Rev. D.01 (Gaussian, Inc.).

Gan, Z., Cao, Y., Evans, R.A., and Gu, M. (2013). Three-dimensional deep sub-diffraction optical beam lithography with 9 nm feature size. Nat.Commun. *4*, 2061. https://doi.org/10.1038/ncomms3061.

Ge, J., Zhang, Q., Jiang, J., Geng, Z., Jiang, S., Fan, K., Guo, Z., Hu, J., Chen, Z., Chen, Y., et al. (2015). Bringing light into the dark triplet space of molecular systems. Phys. Chem. Chem. Phys. *17*, 13129–13136. https://doi.org/10.1039/c5cp00323g.

Harke, B., Bianchini, P., Brandi, F., and Diaspro, A. (2012). Photopolymerization inhibition dynamics for sub-diffraction direct laser writing lithography. ChemPhysChem *13*, 1429–1434. https://doi.org/10.1002/cphc.201200006.

Harke, B., Dallari, W., Grancini, G., Fazzi, D., Brandi, F., Petrozza, A., and Diaspro, A. (2013). Polymerization inhibition by triplet state absorption for nanoscale lithography. Adv.Mater. *25*, 904–909. https://doi.org/10.1002/adma.201204141.

Hell, S.W. (2007). Far-field optical nanoscopy. Science *316*, 1153–1158. https://doi.org/10.1126/science.1137395.

Izakura, S., Gu, W., Nishikubo, R., and Saeki, A. (2018). Photon upconversion through a cascade process of two-photon absorption in $CsPbBr_3$ and triplet–triplet annihilation in porphyrin/diphenylanthracene. J. Phys. Chem. C *122*, 14425–14433. https://doi.org/10.1021/acs.jpcc.8b05508.

Jacopo, P., and Angelo, M. (2017). Recent advances in the application triplet–triplet annihilation-based photon upconversion systems to solar technologies. J. Photonics *8*, 1–16. https://doi.org/10.1117/1.JPE.8.022005.

Kajii, Y., Nakagawa, T., Suzuki, S., Achiba, Y., Obi, K., and Shibuya, K. (1991). Transient absorption, lifetime and relaxation of $C_{60}$ in the triplet state. Chem. Phys. Lett. *181*, 100–104. https://doi.org/10.1016/0009-2614(91)90339-b.

Kasha, M. (1950). Characterization of electronic transitions in complex molecules. Discuss. Faraday Soc. *9*, 14–19. https://doi.org/10.1039/DF9500900014.

Klar, T.A., and Hell, S.W. (1999). Subdiffraction resolution in far-field fluorescence microscopy. Opt. Lett. *24*, 954–956.

Klar, T.A., Jakobs, S., Dyba, M., Egner, A., and Hell, S.W. (2000). Fluorescence microscopy with diffraction resolution barrier broken by stimulated emission. Proc. Natl. Acad. Sci. U S A *97*, 8206–8210.

Knee, J., and Johnson, P. (1985). Lifetimes of dissociation-relaxed triplet states of pyrazine and pyrimidine. J. Phys. Chem. *89*, 948–951. https://doi.org/10.1021/j100252a012.

Krishnan, R., Binkley, J.S., Seeger, R., and Pople, J.A. (1980). Self-consistent molecular orbital methods. XX. A basis set for correlated wave functions. J. Chem. Phys. *72*, 650–654. https://doi.org/10.1063/1.438955.

Kuebler, S.M., Ananthavel, S., Rumi, M., Marder, S.R., Perry, J.W., Barlow, S., Cumpston, B.H., Dyer, D.L., Ehrlich, J.E., Erskine, L.L., et al. (1999). Two-Photon Polymerization Initiators for Efficient Three-Dimensional Optical Data Storage and Microfabrication (IEEE), pp. 107–108.

LaFratta, C.N., Fourkas, J.T., Baldacchini, T., and Farrer, R.A. (2007). Multiphoton fabrication. Angew. Chem. Int. Ed. *46*, 6238–6258. https://doi.org/10.1002/anie.200603995.

Li, L., Gattass, R.R., Gershgoren, E., Hwang, H., and Fourkas, J.T. (2009). Achieving λ/20 resolution by one-color initiation and deactivation of polymerization. Science *324*, 910–913. https://doi.org/10.1126/science.1168996.

Liaros, N., Cohen, S.R., and Fourkas, J.T. (2018a). Determination of the contributions of two simultaneous absorption orders using 2-beam action spectroscopy. Opt. Express *26*, 9492–9501. https://doi.org/10.1364/OE.26.009492.

Liaros, N., Gutierrez Razo, S.A., and Fourkas, J.T. (2018b). Probing multiphoton photophysics using two-beam action spectroscopy. J. Phys. Chem. A *122*, 6643–6653. https://doi.org/10.1021/acs.jpca.8b04463.

Liaros, N., and Fourkas, J.T. (2017). The characterization of absorptive nonlinearities. Laser Photonics Rev. *11*, 1700106. https://doi.org/10.1002/lpor.201700106.

Liaros, N., and Fourkas, J.T. (2019). Ten years of two-color photolithography [Invited]. Opt. Mater. Express *9*, 3006. https://doi.org/10.1364/ome.9.003006.

Liaros, N., and Fourkas, J.T. (2021). Methods for determining the effective order of absorption in radical multiphoton photoresists: a critical analysis. Laser Photonics Rev. *15*, 2000203. https://doi.org/10.1002/lpor.202000203.

Lower, S.K., and El-Sayed, M.A. (1966). The triplet state and molecular electronic processes in organic molecules. Chem.Rev. *66*, 199–241. https://doi.org/10.1021/cr60240a004.

Marenich, A.V., Cramer, C.J., and Truhlar, D.G. (2009). Universal solvation model based on solute electron density and on a continuum model of the solvent defined by the bulk dielectric constant and atomic surface tensions. J. Phys. Chem. B *113*, 6378–6396. https://doi.org/10.1021/jp810292n.

Marian, C.M. (2012). Spin-orbit coupling and intersystem crossing in molecules. Wiley Interdiscip. Rev. Comput. Mol. Sci. *2*, 187–203. https://doi.org/10.1002/wcms.83.

Mueller, J.B., Fischer, J., Mayer, F., Kadic, M., and Wegener, M. (2014). Polymerization kinetics in three-dimensional direct laser writing. Adv. Mater. *26*, 6566–6571. https://doi.org/10.1002/adma.201402366.

Mundt, R., Villnow, T., Ziegenbein, C.T., Gilch, P., Marian, C., and Rai-Constapel, V. (2016). Thioxanthone in apolar solvents: ultrafast internal conversion precedes fast intersystem crossing.

Phys. Chem. Chem. Phys. *18*, 6637–6647. https://doi.org/10.1039/c5cp06849e.

Otis, C.E., Knee, J.L., and Johnson, P.M. (1983). Nonradiative processes in the channel three region of the S1 state of ultracold benzene. J. Phys. Chem. *87*, 2232–2239. https://doi.org/10.1021/j100235a037.

Patterson, L.K., Porter, G., and Topp, M.R. (1970). Oxygen quenching of singlet and triplet states. Chem. Phys. Lett. *7*, 612–614. https://doi.org/10.1016/0009-2614(70)87019-1.

Rai-Constapel, V., Salzmann, S., and Marian, C.M. (2011). Isolated and solvated thioxanthone: a photophysical study. J. Phys. Chem. A *115*, 8589–8596. https://doi.org/10.1021/jp2022456.

Rai-Constapel, V., Villnow, T., Ryseck, G., Gilch, P., and Marian, C.M. (2014). Chimeric behavior of excited thioxanthone in protic solvents: II. Theor. J. Phys. Chem. A *118*, 11708–11717. https://doi.org/10.1021/jp5099415.

Rauch, M.P., and Knowles, R.R. (2018). Applications and prospects for triplet-triplet annihilation photon upconversion. Chimia *72*, 501–507. https://doi.org/10.2533/chimia.2018.501.

Romanovskii, Y.V., Gerhard, A., Schweitzer, B., Scherf, U., Personov, R.I., and Bassler, H. (2000). Phosphorescence of pi-conjugated oligomers and polymers. Phys. Rev. Lett. *84*, 1027–1030. https://doi.org/10.1103/PhysRevLett.84.1027.

Smith, M.B., and Michl, J. (2010). Singlet fission. Chem.Rev. *110*, 6891–6936. https://doi.org/10.1021/cr1002613.

Steiner, U., and Winter, G. (1978). Position dependent heavy atom effect in physical triplet quenching by electron donors. Chem. Phys. Lett. *55*, 364–368. https://doi.org/10.1016/0009-2614(78)87040-7.

Stranius, K., Hertzog, M., and Borjesson, K. (2018). Selective manipulation of electronically excited states through strong light-matter interactions. Nat.Commun. *9*, 2273. https://doi.org/10.1038/s41467-018-04736-1.

Stromqvist, J., Chmyrov, A., Johansson, S., Andersson, A., Maler, L., and Widengren, J. (2010). Quenching of triplet state fluorophores for studying diffusion-mediated reactions in lipid membranes. Biophys.J. *99*, 3821–3830. https://doi.org/10.1016/j.bpj.2010.09.059.

Sugioka, K., and Cheng, Y. (2014). Femtosecond laser three-dimensional micro- and nanofabrication. Appl. Phys. Rev. *1*, 041303. https://doi.org/10.1063/1.4904320.

Szabó, A., and Ostlund, N.S. (1982). Modern Quantum Chemistry: Introduction to Advanced Electronic Structure Theory (Macmillan).

Tomova, Z., Liaros, N., Gutierrez Razo, S.A., Wolf, S.M., and Fourkas, J.T. (2016). In situ measurement of the effective nonlinear absorption order in multiphoton photoresists. Laser Photonics Rev. *10*, 849–854. https://doi.org/10.1002/lpor.201600079.

Villnow, T., Ryseck, G., Rai-Constapel, V., Marian, C.M., and Gilch, P. (2014). Chimeric behavior of excited thioxanthone in protic solvents: I. Experiments. J. Phys. Chem. A *118*, 11696–11707. https://doi.org/10.1021/jp5099393.

Wolf, T.J., Fischer, J., Wegener, M., and Unterreiner, A.N. (2011). Pump-probe spectroscopy on photoinitiators for stimulated-emission-depletion optical lithography. Opt. Lett. *36*, 3188–3190. https://doi.org/10.1364/OL.36.003188.

Yang, Z., Mao, Z., Xie, Z., Zhang, Y., Liu, S., Zhao, J., Xu, J., Chi, Z., and Aldred, M.P. (2017). Recent advances in organic thermally activated delayed fluorescence materials. Chem. Soc. Rev. *46*, 915–1016. https://doi.org/10.1039/c6cs00368k.

Yang, L., Münchinger, A., Kadic, M., Hahn, V., Mayer, F., Blasco, E., Barner-Kowollik, C., and Wegener, M. (2019). On the Schwarzschild effect in 3D two-photon laser lithography. Adv. Opt. Mater. *7*, 1901040. https://doi.org/10.1002/adom.201901040.

Zhao, H., and Mazumdar, S. (2004). Electron-electron interaction effects on the optical excitations of semiconducting single-walled carbon nanotubes. Phys. Rev. Lett. *93*, 157402. https://doi.org/10.1103/PhysRevLett.93.157402.

Zhao, Y., and Truhlar, D.G. (2011). Applications and validations of the Minnesota density functionals. Chem. Phys. Lett. *502*, 1–13. https://doi.org/10.1016/j.cplett.2010.11.060.

Zhao, J., Wu, W., Sun, J., and Guo, S. (2013). Triplet photosensitizers: from molecular design to applications. Chem. Soc. Rev. *42*, 5323–5351. https://doi.org/10.1039/c3cs35531d.

# STAR★METHODS

## KEY RESOURCES TABLE

| REAGENT OR RESOURCE | SOURCE | IDENTIFIER |
|---|---|---|
| Chemicals, peptides, and recombinant proteins | | |
| Isopropylthioxanthone | Sigma Aldrich | CAS Number: 75081-21-9 |
| Pentaerythritol triacrylate | Sartomer | CAS Number: 4986-89-4 |
| Software and algorithms | | |
| Gaussian09 suite of programs | Gaussian, Inc. | http://gaussian.com |
| SigmaPlot 14.0 | Systat Software | https://systatsoftware.com |

## RESOURCE AVAILABILITY

### Lead contact

Further information requests should be directed to the lead contact, Professor John T. Fourkas (fourkas@umd.edu).

### Materials availability

This study did not generate new unique reagents.

### Data and code availability

Any data and analytical methods that are not reported numerically in the main text or in the supplemental information section are available from the lead contact upon request. This study did not generate any unique code.

## METHOD DETAILS

### Substrate functionalization

#1 Corning glass coverslips (25 mm × 25 mm), were cleaned in an oxygen plasma for 3 min, then immersed overnight (16 h) in a solution of 93% anhydrous ethanol (Pharmco-Aaper), 5% deionized water and 2% (3-acryloxypropyl) trimethoxysilane (Gelest). The functionalized substrates were rinsed in ethanol for 1 h and dried in an oven at 95°C for 1 h.

### Photoresist preparation

The photoresist samples were made by adding the specified weight percent of ITX to pentaerythritol triacrylate (PETA) or trimethylolpropane triacrylate (TMPTA) monomers. All samples were heated for 5 minutes in a 55°C oven, and then were mixed at 2350 rpm for 5 min using a centrifugal mixer. This procedure was repeated until the resins formed homogeneous dispersions. After mixing, a drop of the photoresist was placed on a functionalized, #1 glass coverslip.

### 2-BIT measurements

A tunable, ultrafast Ti:sapphire oscillator (Coherent Mira 900-F) was used as the excitation source. The repetition rate of the laser was 76 MHz, and the pulse duration was ~150 fs. The beam was spatially filtered and then split into two portions of roughly equal average power. To adjust the power of each beam we employed a motorized half-wave plate and a Glan-Taylor polarizer. The two pulse trains were combined by means of a polarizing beam cube and made collinear. The timing between the two pulse trains was controlled by a delay line, so that consecutive pulses arrived at the sample with roughly equally spaced timings, and the effective repetition rate was 152 MHz. The beams were sent through the reflected-light illumination port of an inverted microscope and were focused using a 100×, 1.45-NA oil-immersion objective (α Plan-FLUAR, ZEISS), the back aperture of which was overfilled. Each beam was passed through a separate variable beam expander to allow for adjustment of the beam size at the back aperture of the microscope objective. Samples were mounted on a 3-axis piezoelectric stage (Physik Instrumente) for

nanopositioning in all dimensions. The piezo stage was attached to a motor-driven stage (Ludl Electronic Products, Ltd) for coarse sample positioning. The movement of the sample stage was controlled using custom-made LabVIEW (National Instruments) programs, and fabrication was monitored in real time using a CCD camera and a display. For the proper alignment and overlapping of the point-spread functions of the two laser beams, gold nanoparticles were coated onto a cover slip from a dilute solution. Once a nanoparticle was located at low magnification from its multiphoton absorption induced luminescence (MAIL) signal (Farrer et al., 2005). The laser focal point from the 100× objective was scanned over the gold nanoparticle using the piezo stage, either in the *xy* or *xz* planes. The signal was collected by a single-photon-counting avalanche photodiode (EG&G Canada) and was transferred to a computer by a data-acquisition board (National Instruments). Data collection was performed by a program written in LabVIEW. The first step in a 2-BIT measurement is to determine the polymerization threshold average powers of each pulse train independently. These thresholds were measured by focusing the laser beam inside the photoresist and creating sets of lines at a stage velocity of 20 μm/s. The minimum average power at which fabricated lines were observed was then determined visually on the display screen. During all measurements, the axial position of the focal plane was kept fixed to ensure that a constant distance was maintained above the coverslip surface. This restriction is important, because any change in the focal plane inside the photoresist may affect the determination of the threshold exposure.

To increase the power measurement accuracy, a reflected part of the beam (~5%) was chopped at a fixed frequency and was sent to a calibrated Si photodiode, the output of which was sent to a lock-in amplifier (Stanford Research Systems, SR810) referenced to the chopping frequency. The power of the first laser beam was then lowered to a set of fixed values below the threshold. For each of the fixed values of the average power of beam 1 ($P_1$), the corresponding minimum value of the average power of the second beam ($P_2$) for which polymerization was observed at the same stage velocity was determined. The values of $P_1$ were chosen so that a representative range of values of $P_2$ was measured, such that the plot of $\overline{P}_1$ vs. $\overline{P}_2$ could be fit reliably. Here the overbars indicate the average power normalized to the threshold average power for that beam alone. At least five measurements were made for each set of average powers so that reproducibility could be quantified. The obtained data were fitted to the equation

$$\overline{P}_1^n + \overline{P}_2^n = 1. \qquad \text{(Equation S1)}$$

Because data points near the diagonal of a 2-beam action spectroscopy plot are more indicative of the value of *n*, we used a fit weighting for each point of

$$w = \frac{1}{0.05 + |\overline{P}_1 - \overline{P}_2|}. \qquad \text{(Equation S2)}$$

## 2-BCEIn measurements

The same two-beam arrangement and alignment procedure was used as in the 2-BIT experiments. A 200 μL sample of 2 wt% ITX in PEG-400 was placed in a custom-made Teflon cell with #0 glass coverslips for windows. The cell was mounted on a three-axis piezoelectric stage for fine sample positioning in all dimensions. The piezo stage was attached to a motor-driven stage for coarse sample positioning. The movement of the piezo stage was controlled using a LabVIEW program. To avoid photobleaching during the fluorescence experiments, the piezo stage was moved constantly in a circle with a radius of 20 μm at a velocity of 50 μm/s. This speed is fast enough to prevent immediate photobleaching and slow enough to permit diffusion away from the beam path between subsequent scans over the same spot. The relative positions of the two focal spots in the sample were determined by monitoring the nonlinear fluorescence excitation signal of each beam using a CCD camera. To avoid any inner filter effects, the beams were focused near the surface of the cell, and an epifluorescence geometry was used to collect the emission. The fluorescence was detected by a silicon photodiode (Thorlabs SM1PD1A), the output of which was sent to an analog, low-noise preamplifier (Stanford Research Systems, SR560), and then to a lock-in amplifier (Stanford Research Systems, SR810) referenced to the chopping frequency. Appropriate short-pass filters were used to prevent any excitation laser light from being sent to the photodiode. The average power values cited here were measured with a power meter at the back aperture of the objective (α Plan-FLUAR, ZEISS) with the chopper running. The additional loss from the objective was ~30%. No autofluorescence was observed from solvent blanks at any excitation wavelength used here.

### 2-color luminescence excitation/deactivation measurements

A tunable, ultrafast Ti:sapphire oscillator (Coherent Mira 900-F) was used as the excitation source. A second, identical laser oscillator was used in CW mode for inhibition of luminescence. The procedure for the overlapping of the two beams is the same as described for 2-BIT above. A 200 μL sample of 2 wt% ITX in PEG-400, was placed in a custom-made Teflon cell with #0 glass coverslips for windows. The sample mounting and detection geometry were similar to those in the 2-BCEIn experiments. Only the ultrafast beam (excitation) was chopped, and the photodiode signal was sent to a preamplifier (Stanford Research Systems, SR560), and then to a lock-in amplifier (Stanford Research Systems, SR810). The excitation and deactivation beams were overlapped using a polarizing beam cube. In all experiments, the neat solvent was found to have no measurable nonlinear fluorescence signal. For the fitting of the experimental data and extraction of the order of nonlinearity the same procedure was used as for the 2-BIT data.

### *In situ* measurements of polymerization and deactivation

The fundamental components of the experimental setup are shown in Figure S10A. The activation wavelength was 315 nm and the deactivation wavelength was 630 nm. A sample of 0.5 wt % ITX in PETA was prepared in a thick film between a cover slip and an acrylated cover slip. The sample was irradiated with a series of the two colors of pulsed light and the deactivation threshold was measured as a function of delay time. The light used in this experiment was generated by a Continuum Horizon optical parametric oscillator (OPO) pumped by the third harmonic of an Nd:YAG. The linearly polarized pulses were ~7 ns in duration with a wavelength resolution of < 0.01 nm. The 630 nm output of the OPO was sent into an Inrad doubler to generate 315 nm pulsed light that propagated collinearly with the 630 nm pump beam. A 315 nm high reflector was used to separate the two beams into two distinct beam paths. The 630 nm beam traversed a delay line and was recombined collinearly with the 315 nm beam, allowing the time between the activation and deactivation pulses to be varied from 0 to 20 ns. The thick-film sample was positioned in the *xy*-plane and the beams propagated along the *z*-axis, normal to the surface of the glass slide. This geometry is illustrated in Figure S10B. After irradiation, the sample was developed with ethanol to establish the presence of crosslinking. At a set delay time and activation energy, the deactivation beam power at which complete deactivation occurred was determined. The energy of the deactivation beam was decreased in increments of 0.2 mJ/pulse for each consecutive sample, and the deactivation threshold was measured when evidence of polymerization was clear to the naked eye after development.

### Microsecond transient absorption

Microsecond time scale transient absorption studies were conducted using the frequency tripled, 355 nm output of a Nd:YAG laser (Continuum) with pulses of 4 to 6 ns in duration as the excitation source. The probe was a 350 W xenon arc lamp that passed through a monochromator to a PMT detector. Samples were prepared such that the optical density at 355 nm was between 1.0 and 2.0. Solutions were purged with nitrogen gas both in the solution (minimum of 10 min) and in the headspace (minimum of 5 min). When obtaining a full spectrum, a fresh supply of the sample was delivered into the cuvette via a nitrogen-purged flow cell that connected the cuvette to the stock solution via a double-headed needle. The photolyzate was drained from the cuvette into a waste vessel. This setup prevents accumulation of photoproducts and avoids the depletion of the ITX throughout the duration of the experiment.

### Ultrafast pump-probe spectroscopy

The ultrafast transient absorption spectra were recorded using an ultrafast pump/probe spectrometer (Newport Corporation). A Ti:sapphire amplified laser produced laser pulses of < 50 fs duration and ~1 mJ pulse energy at center wavelength of 800 nm, with a repetition rate of 1 kHz. A small part of the fundamental laser beam was used to generate white light continuum in $CaF_2$. The remaining portion of the beam was frequency-doubled using a BBO crystal, and any residual 800 nm light was removed using a shortpass filter. The frequency-doubled beam was used as the pump, and was chopped at 500 Hz. The white light supercontinuum beam was used as the probe, and could be temporally delayed with respect to the pump by up to 4.3 ns. The two beams were focused and overlapped in the sample. The sample was stirred in a 2-mm-path-length cuvette and measured 0.014 OD at 400 nm and 0.206 OD at 381 nm. The images of the signal and reference probe beams were concurrently recorded as a function of delay time between the pump and the probe, by means of a CMOS photodiode-array based camera mounted at the exit of a spectrograph. The spectrograph was capable of data acquisition at a rate of 1 to 10 kHz data acquisition, or even

higher with multiple pulses averaged per acquisition. To increase resolution, in each scan 4 s of averaging per time point was used, and two scans were averaged.

## Density functional theory calculations

Geometry optimizations and energy calculations were carried out using the Gaussian09 suite of programs (Frisch et al., 2009). Structures were optimized using (U)M06-2X/6-311G(d) (Krishnan et al., 1980; Zhao and Truhlar, 2011). For calculations carried out in solvents, the SMD solvation model was used (Marenich et al., 2009). Energies of the electronic states were calculated using TD-DFT. A detailed summary of the results of the DFT calculations is given in the supplemental information (Figures S4–S8).

## Details of the kinetic model

For simplicity, we assume temporally square excitation pulses. If the excitation beam has average irradiance $I$, then the peak irradiance is $I/D$, where $D$ is the duty cycle (i.e., the pulse duration divided by the repetition time). Given a total exposure time of $t'$, the laser field is on for time

$$t = Dt'. \qquad \text{(Equation S3)}$$

Thus, the total linear exposure dose is given by the peak irradiance multiplied by the exposure time

$$\frac{I}{D} \cdot Dt' = It'. \qquad \text{(Equation S4)}$$

This result is relevant to linear absorption. For the case of 2-photon absorption, the total exposure dose is given by the product of the square of the peak irradiance and the exposure time

$$\left(\frac{I}{D}\right)^2 \cdot Dt' = \frac{I^2 t'}{D}. \qquad \text{(Equation S5)}$$

Based on the scheme in Figure 4A and these equations, the rates of change of the populations of the $S_0$ and $T_1$ states are

$$\frac{d[S_0]}{dt} = -\frac{k_2 I^2}{D}[S_0] + k_1 I[T_1]. \qquad \text{(Equation S6)}$$

and

$$\frac{d[T_1]}{dt} = \frac{k_2 I^2}{D}[S_0] - k_1 I[T_1]. \qquad \text{(Equation S7)}$$

Conservation of population implies that

$$[S_0]_0 = [S_0]_{t'} + [T_1]_{t'}. \qquad \text{(Equation S8)}$$

Substituting this constraint into Equation S4 and integrating yields

$$[S_0]_{t'} = \frac{[S_0]_0}{k_1 I + \frac{k_2 I^2}{D}}\left(k_1 I + \frac{k_2 I^2}{D}\exp\left[-\left(k_1 I + \frac{k_2 I^2}{D}\right)t'\right]\right). \qquad \text{(Equation S9)}$$

The corresponding triplet population is

$$[T_1]_{t'} = \frac{[S_0]_0 \frac{k_2 I^2}{D}}{k_1 I + \frac{k_2 I^2}{D}}\left(1 - \exp\left[-\left(k_1 I + \frac{k_2 I^2}{D}\right)t'\right]\right). \qquad \text{(Equation S10)}$$

Dividing both sides of Equation S10 by $[S_0]_0$ yields Equation 2. When a CW deactivation beam with irradiance $I_d$ is also present, $k_1 I$ in the above equations is replaced with $k_1(I + I_d)$.

At $t' = \infty$, the threshold concentration of $T_1$ is

$$[T_1]_{th,\infty} = \frac{[S_0]_0 \frac{k_2 I^2}{D}}{k_1 I + \frac{k_2 I^2}{D}}. \qquad \text{(Equation S11)}$$

The corresponding value of the threshold irradiance at the fundamental frequency is

$$I_{th,f} = \frac{Dk_1[T_1]_{th,\infty}}{k_2\left(1 - [T_1]_{th,\infty}\right)}. \quad \text{(Equation S12)}$$

If the repetition rate is doubled, the threshold triplet concentration at equilibrium remains constant. Therefore,

$$I_{th,2f} = \frac{2Dk_1[T_1]_{th,\infty}}{k_2\left(1 - [T_1]_{th,\infty}\right)}. \quad \text{(Equation S13)}$$

Along the diagonal in a 2-BIT experiment, the irradiance for each pulse train is the same, and therefore we must divide the result in Equation S13 by 2, recovering Equation S12. The 2-BIT exponent $m$ in this case is given by (Cohen and Fourkas, 2019)

$$m = \frac{\ln(1/2)}{\ln(1)} = \infty. \quad \text{(Equation S14)}$$